Video Analysis of Small Vulcanian Explosions at Santiaguito, Guatemala

By

R. Adam Blankenbicker

A THESIS

Submitted in partial fulfillment of the requirements

for the degree of

MASTER OF SCIENCE in GEOLOGY

MICHIGAN TECHNOLOGICAL UNIVERSITY

2009

This thesis, “Video Analysis of Small Vulcanian Explosions at Santiaguito, Guatemala” is hereby approved in partial fulfillment of the requirements for the Degree of MASTER OF SCIENCE in Geology

DEPARTMENT:

Geological and Mining Engineering and Sciences

Signatures:

Thesis Advisor:_____

William I. Rose

Department Chair:_____

John S. Gierke

Date:_____

Table of Contents

Abstract

During two extended periods (July-September, 2007 and January-March, 2008) we recorded and analyzed 31 small explosions at Santiaguito Volcano, Guatemala, including time-height relations and cloud dimensions. Volcanic plumes at Santiaguito result from the unsteady emissions of ash and gas through concentric ring fractures and a series of smaller fractures within the rings in the dome. Observations from the summit of Santa Maria reveal three principle components to the resulting explosion clouds; steady explosions of gas with variable amounts of ash, passive emissions of gas, and brief (<10 seconds) bursts of ash-rich jets which collapse upon themselves. Explosions lasted 30-300 seconds and occurred every 15-150 minutes. They consisted of 1-8 pulses and typically reached heights of 800-1500m above the vent. The first 1 or 2 observable pulses in each explosion typically had the lowest near-vent velocities (4-16m·s^{-1} at <100m above vent) and higher velocities were measured in later pulses higher above the vent. At low heights above the vent later pulses were masked by previous pulses, but their higher velocities at higher elevations, where they were visible, suggest they had higher initial velocities than earlier pulses. Explosions end with a degassing stem that slowly wanes. This suggests that the vent system opens gradually in increments before it closes and reseals. Typical eruption rate for the analyzed explosions was on the order of 130-3500kg s^{-1} and the gas mass fraction is large, about 0.19 for average explosions. The explosion clouds we observed are similar to those described at other volcanoes with distinct eruption mechanisms. Through this reasoning, explosions at Santiaguito can be classified as low-intensity vulcanian.

Introduction

Understanding the source conditions that drive volcanic explosions is necessary in determining the potential threat an eruption may pose. This is especially important for open vent systems because local populations may be accustomed to low-level volcanic activity and therefore will not respond appropriately to changes in the activity.

Detailed video analysis of volcanic activity has been used in previous studies of small to moderate scale eruptions at open-vent systems. At Soufriere Hills Volcano, Montserrat (Formenti et al., 2003) magmatic water content, bulk densities of jets and fragmentation pressure were estimated with only measurements of velocity and initial radius. At Asama and Miyakejima, in Japan, (Terada and Ida, 2007) measurements of radii of discrete thermals and their height over time were used to calculate air entrainment into plumes and thermals using models developed by Morton (1956), Scorer (1957), and Turner (1964). Thermal video has also been used (Patrick, 2007; 2007a; Patrick et al., 2007b) to describe dynamic and morphologic characteristics of thermals, plumes and jets at Stromboli volcano, Italy, to provide insight into the source conditions of Strombolian-type eruptions. Video analysis is also helpful in qualitative measures. The ability to watch an explosion cloud, flowing magma or vent processes in forward and reverse at various speeds aids in describing the "how" of a process (Patrick, 2007).

Santiguito has displayed explosions, similar to those observed in this study, nearly every day since 1968 (Rose et al., 1970; Smithsonian Global Volcanism Program, http://www.volcano.si.edu/). The current accepted model of eruptive activity at Santiaguito includes a dacitic plug which moves unsteadily in stick-slip movements, causing vertically directed explosions of gas and ash to occur within and around a ring-shaped vent (Bluth and Rose, 2004; Johnson et al., 2008; Sahetapy-Engel et al., 2008). Shearing against the conduit wall causes gas to decouple from the magma and accounts for the high gas content released in the explosions which rise buoyantly (Bluth and Rose, 2004; Johnson et al., 2004). Explosions end as the system reseals itself and gas emission rates drop (Branan, 2007; Dalton, Personal Communication, 2009).

In this report we analyze the onset and evolution of small explosions at Santiaguito. We use video analysis to constrain probable eruption rates by measuring velocity, height and plume dimensions through time. Using our measurements in commonly used models (e.g. Sparks et al., 1997; Settle, 1978), we were able to constrain the probable eruptive rates required for buoyantly-rising plumes that achieved heights of up to 1800-1900m above the vent. We also characterize the dynamics of these explosions and describe how they compare with eruption mechanisms proposed by other recent studies (Bluth and Rose, 2004; Johnson et al., 2008; Sahetapy-Engel et al., 2008; 2009).

Past Effusive and Explosive Activity at Santiaguito

The Santiaguito Dome complex has experienced dome extrusion since its inception in 1922 but the lava extrusion is unsteady on a range of time scales. High extrusion rates (1-3 $m^3 sec^{-1}$) which last 3-5 years alternate with longer periods (5-15 years) of much lower (0.1-0.4 m^3 sec^{-1}) extrusion rates (Rose, 1973; 1987; Harris et al 2003). Santiaguito has extruded about 1.5-2 km^3 of dacite since 1922, and since 1999 extrusion has been occurring at a slow (<0.3m^3 sec^{-1}) and decreasing rate (Harris et al, 2004; Durst et al, in review). Although activity began at the Caliente vent, and is currently focused there, a brief shift in the activity led to formation of 3 other endogenous domes trending westward: La Mitad, El Monje, and El Brujo (Rose, 1972; Harris et al., 2002) (Figure 1). Since 1975 activity at Santiaguito has shifted completely back to the Caliente vent, where the early dome units extruded in 1922-29 have now been nearly completely covered by much younger block lava flows (Escobar et al., in press).

Aster-derived extrusion rate estimates for Santiaguito by Bowman (2008), following methods of Harris et al. (2003), show 2006-2008 levels that are generally lower than 0.2 $m^3 sec^{-1}$. Magma extrusion led to the formation of a ~200m long lava flow towards the SW flank whose flow front continually fragmented and caused small rock falls which showed no correlation with the vertical explosions.

Explosive activity at Santiaguito has remained nearly constant since 1968 (Rose et al., 1970; Smithsonian Global Volcanism Program, http://www.volcano.si.edu/, Current). Explosions of ash and gas have occurred at rates of 0.1-5 per hour and have typically achieved heights of 500-

2,000m above the vent (2,500m asl). Occasional large explosions have reached 4-5km above the vent. Since 2000 extrusion through the Caliente vent has been observed as unsteady with sudden plug-like extrusions accompanied by explosions with reposes that last about 0.5 to 2 hr (Bluth and Rose, 2004; Johnson et al., 2008, Sahetapy-Engel et al., 2008).

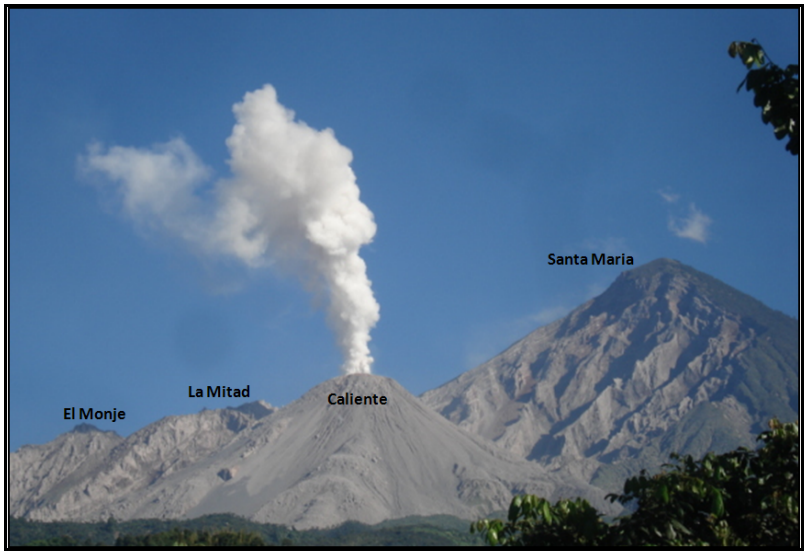

Figure 1. Erupting Caliente vent, La Mitad, El Monje and Santa Maria from OVSAN, Feb. 4, 2008. El Brujo is out of view, W of El Monje. Explosion is sustained release of gas and little ash, indicated by its white color. Explosion was not recorded on video.

Methodology

During two extended periods (described in Table 1) video was recorded (30fps) from the Santiaguito Volcano Observatory, OVSAN, located 6km south of the Caliente vent (Figure 2). We could only observe the volcano for about 2-5 hours a day before atmospheric clouds moved in, covering the volcano. Due to this limited window there were several days where only one explosion (or no explosions) was observed and no repose time could be calculated. Explosions were analyzed with a freeware program, *Tracker* (Brown, www.cabrillo.edu/~dbrown/tracker/) that allows mapping the position and dimension of a mobile object or body through time in 2-dimensional space (Figure 3). In Tracker an X-Y axis is placed onto the fixed video image which includes the Caliente vent and Santa Maria. The X-axis, marked by the horizontal red line in Figure 3, is placed directly on top of the active Caliente vent, marking this height, Z, as 0m. Through scaling and

perspective corrections (detailed in appendix), when the top of an explosion is in line with the summit of Santa Maria, this is an equivalent of 436m above the vent.

Table 1. Dates of observation periods when explosions were recorded with digital video camera

Period	Observation Dates	Number of Explosions Analyzed
1	Jul. 01, 2007 – Sep. 25, 2007	17
2	Jan. 22, 2008 – Mar. 25, 2008	14

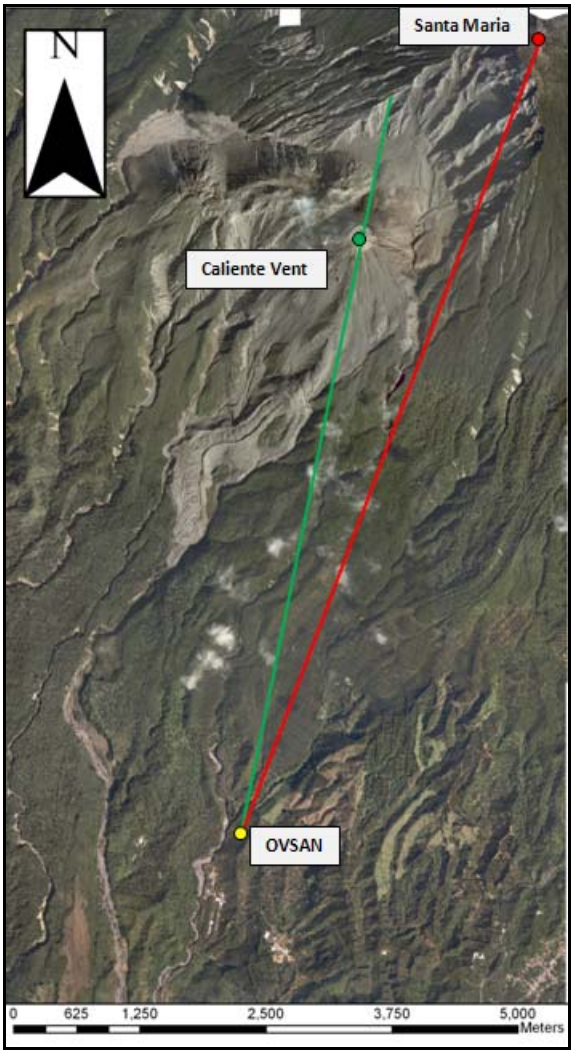

Figure 2. Aerial photo compilation of area including OVSAN (yellow circle, 900masl), Santiaguito (Caliente Vent; green circle, 2,500m asl) and Santa Maria (red circle, 3,772masl). Green line indicates the line of site from OVSAN to the Caliente vent and the red line to the summit of Santa Maria. Compiled from pictures taken Nov. 2005 - Apr. 2006 by JICA.

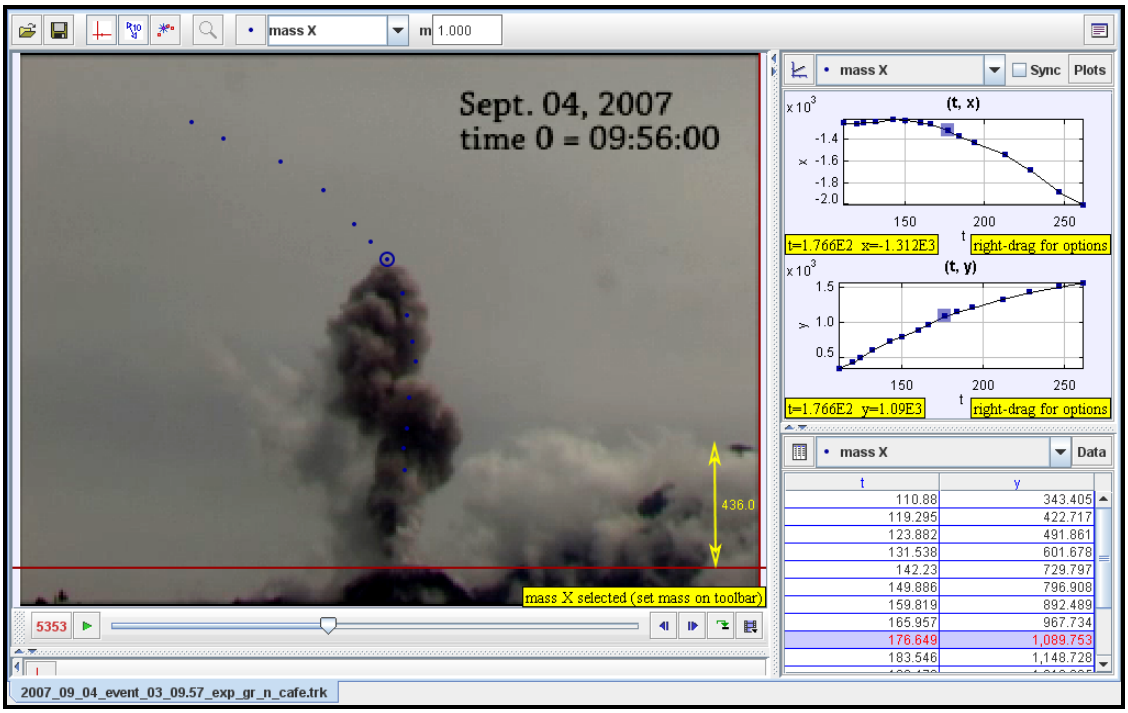

Figure 3. Tracker screen with 2 observable pulses. Pulses are identified by their independent leading edges; one at ~1,100m above the red line, and the other at ~600m. Blue dots represent the location of the leading edge of the higher pulse. The yellow, double-arrowed line measures the 436m from the red line (X-axis, height = 0m) to the summit of Santa Maria (described in more detail in appendix).

Plumes were tracked from when they were first visible until they were obscured by another pulse that over took it, or until the cloud began to move horizontally as result of the wind. In two instances the plume rose above the field of view so the maximum height could not be observed. The maximum heights we were able to measure were recorded as the maximum height the explosion achieved. Average velocity was calculated between two consecutive tracked points (Figure 3). Individual points could be placed very closely, so we were able to accurately measure velocity in small increments over a large distance. Because we were not limited by a small quantity of sensors, improved measurements were made from the methods of Johnson et al. (2004) and Sahetapy-Engel et al. (2008) who used multiple thermal infrared sensors with a limited field of view (1°) aimed at two heights above the vent.

Explosion pulses resulted in two possible forms: 1.) a cloud that rises independently or semi-independently from other clouds (Figure 3) or 2.) a sudden increase in the flux of erupted material that follows the same rise path of the material previously erupted. Pulses were distinguished from each other by either a visible leading edge (as seen in Figure 3) or through the analysis of the progression of height and velocity over time. Figure 4 plots rise velocity of the upper edge of explosion clouds against their height. The top shows the height with time and the bottom shows the velocity. Small kinks are visible in an otherwise gentle arc, which we interpret as the result of a new pulse of activity which has overtaken an earlier pulse. In Figure 4 (bottom), these kinks correlate with spikes in velocity. Each explosion that displayed these characteristic kinks and spikes was interpreted to contain multiple pulses.

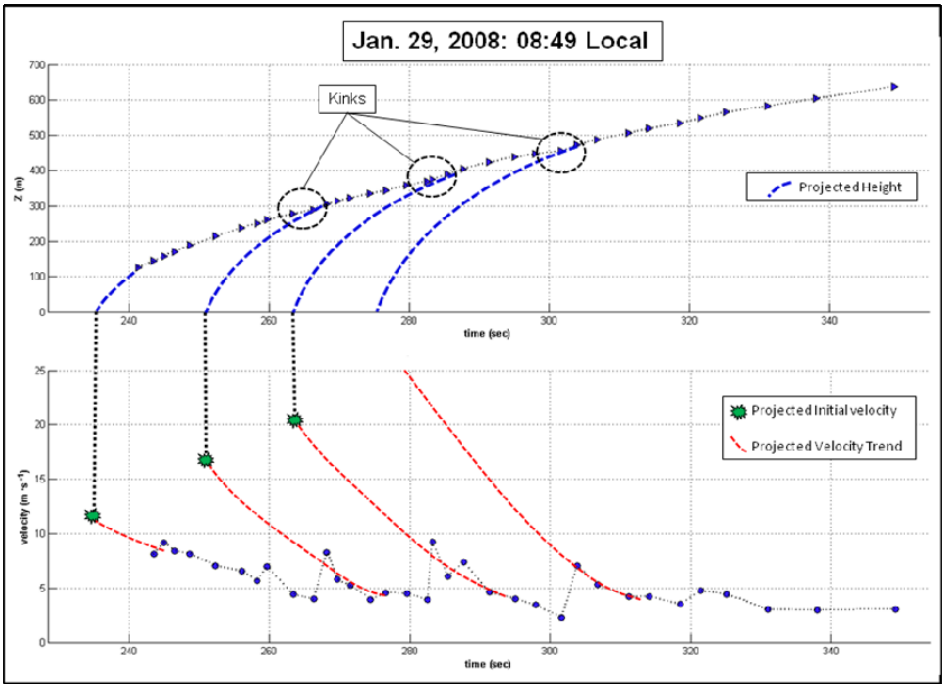

Figure 4. Plot showing the explosion cloud height measurements (above) and velocity (below) after video geometric correction using *Tracker*. This example illustrates how individual pulses were identified in all the explosions. Kinks in the time-height arc and spikes in the time-velocity series are interpreted to indicate multiple pulses. The beginnings of later pulses are often not visible at lower elevations due to masking, and are only visible after they rise above the preceding pulse. Labeled time is from the start of video, not from initiation of explosion.

Results

Small to moderate explosions occurred at intervals of 15 min to 2 hours (average: 50 min) and contained varying quantities of hot ash (grey to brown) and gas (white to blue). They typically lasted (from first observation of cloud until end of major degassing) 30-300 seconds (average: 160 sec) and most resembled continuous emissions that pulsated. Maximum measured heights were approximately 650-1900 m per explosion (mean = 1125 m). Relative ash contents were estimated based on the color and opacity of the plumes. In most cases, the first 2 or 3 pulses in an eruption were ash-rich. Subsequent pulses were lighter in color, suggesting they contained less ash, though masking may have prevented observation of ash in later pulses at lower heights. Local light ashfalls were common, indicating that ash is a common component in many explosions, even though there were some explosions that appeared to be dominated by gas based upon their white color, though it is noted that variable condensation levels affect the color. No bombs or ballistics were visible from OVSAN, but these have been reported in written observations made from closer locations (Bluth & Rose, 2004; Johnson et al, 2004).

At-Vent Observations from Santa Maria

It is understood that because our measurements were made from below the summit of the Caliente vent we could not determine the exact location in the vent where certain smaller scale events occurred. We could only be accurate in measuring in two dimensions; up-down, and east-west – not how far forward or back within the vent. However, video taken in 2002-2004 from the summit of Santa Maria captures the initiation of explosions at the Caliente vent and where within the vent they occur.

For one example (Jan. 11, 2003) the initial emissions (Figure 5, A) began along an inner annular fracture (outlined by inner dashed red circle). The strength of the emission along this fracture was not constant; some locations discharged vigorous clouds while other sections gradually opened to release weak, linear clouds which became more

vigorous with time. After some time the emissions propagated outwards and became more vigorous (B-D). In image B, vertically-directed jets of ash are visible in the northern half of the vent (blue arrows show direction of movement, outlined by dashed blue line). They only lasted briefly and quickly collapsed due to lack of buoyancy. Smaller ash-rich jets are seen in the north-east part of the vent (B, C). It was not possible to locate the sources of these jets because previously erupted material blocked viewing. The momentum-driven rise of all jets did not appear to affect the overall dynamics of the plume, but the material was later incorporated after they collapsed, entraining and heating atmospheric air to become buoyant. Emissions of gas and ash that originally were focused along the center annulus began to propagate towards the outer limits of the vent (light blue arrows). As the activity spread outwards, an outer ring began to open (brown and purple dashed lines, image C). When the activity reached the edge of the vent (C) the north-east section of the outer ring (brown dashed line) powerfully expelled gas and ash vertically which was incorporated into the overall resulting plume. Further south along this segment (dashed purple line) the gas emissions were weaker and there was considerably less ash discharged. A measure of the weakness of these linear emissions is emphasized by the horizontal, not vertical, movement of the gas (purple arrows, C & D) towards the center of activity due to a vacuum effect that had resulted from the rising plume. Small jets of ash along this outer ring caused small pyroclastic flows that fall down the north-east flank a short distance (outlined by green dashed line). The ash that rose from this flow was also incorporated into the plume (C). The collapse of the ash-rich jets (blue dashed line) created a small pyroclastic surge along the north-west section of the vent. This material also became incorporated into the plume as it was sucked by in by the vacuum effect. As the explosion began to end (D), more of the outer ring was visible, defined by the outline of the base of the rising material at the north-west (yellow dashed line). Emissions that were previously directed upwards along the outer ring forcefully (C) weakened over time and subsequently were sucked inwards horizontally due to the vacuum effect (D).

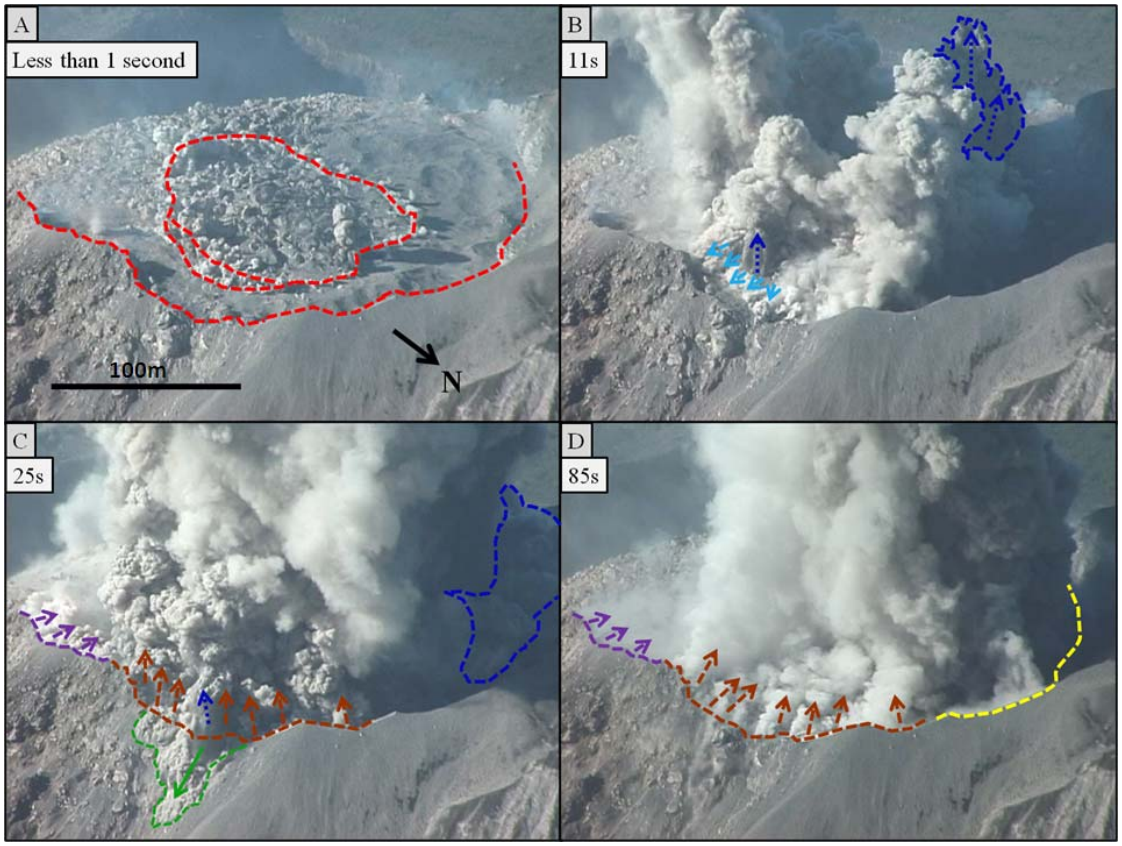

Figure 5. Sequence of an explosion on January 11, 2003, 08:40 local time. Red dashed lines represent major visible fractures observed throughout the explosion. Dashed arrows represent direction of movement of material. Descriptions in text. It is noted that this explosions occurred about 5 years before the current study and therefore does not characterize the explosions studied during this study. This example only serves to describe the components of the explosion clouds.

At-Vent Observations from OVSAN

From OVSAN, it was not possible to observe the details of how the activity propagated along the ring structures within the vent; only the width of the base of the plume could be measured. This measurement is here forth referred to as the initial diameter (D_0). Most events began as a small, weak expulsion of gas or a combination of ash and gas that appeared to exit from a small section of the vent typically about 50m east of the western edge of the horizontal top of Caliente (Figure 6, a.i, b.i). This could correspond to the explosion initiating along the inner annulus or at a point along the annulus somewhere along the north or south edge. Initial diameters were measured 25-190m. Larger initial diameters are recorded for explosions that initiate throughout both annuli.

Pulses with initial diameters of 30-60m were both ash rich and ash poor (range of color from white to grey), whereas those that had initial diameters greater than 60m were all ash-rich (dark grey), and those smaller than 30m contained little to no ash (white to light grey). In many of the explosions, the initial diameter extended eastward a further 50-100m, though the eastern most section was not as impulsive or as ash rich as the west. We could not measure the initial diameter of all individual pulses due to masking by previously erupted pulses. Initial diameter was measured as the distance from the furthest left to furthest right from our perspective.

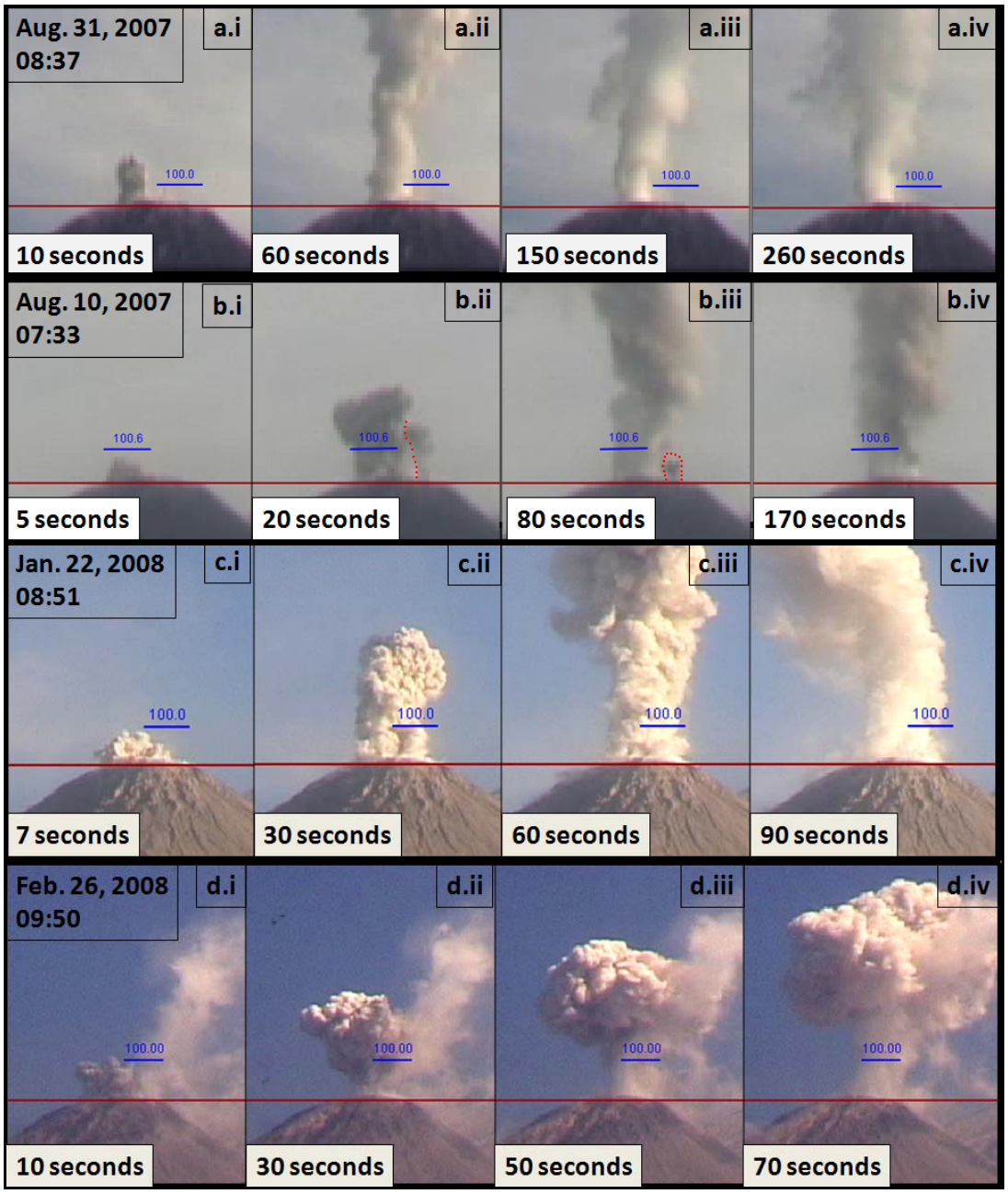

Figure 6. Showing the variation in morphologies. Horizontal red line is the X-axis used in *Tracker* to define height (z) = 0m. Horizontal blue line represents scale of 100m. Left is east, right is west. Time is measured since the initiation of the explosion which began when the explosion was first visible.

Explosions with multiple pulses demonstrated a pattern where at the initiation of a pulse, the initial diameter would reach a maximum and over time would decrease as the emissions momentarily lapsed until another pulse initiated causing the initial diameter to increase again (seen well in Figure 6, bii-iv, highlighted be dashed red line). With the

exception of the explosion example ‘e’ in Figure 6, there was always a stem of ash and gas that attached the leading body of a pulse to the vent that slowly diminished as the explosion concluded. In all events recorded by video, the tail end of the explosions died off at, or very near to, the same location where the initial emissions occurred. This was typically near the central-west side of the vent.

Cloud Morphology

Cloud morphology was variable. Individual explosions consisted of multiple pulses of variable widths that contained variable quantities of ash and gas. Pulses that started with a wide base were more ash-rich and expanded more as they rose than ash-poor pulses. The variable morphology of common explosion clouds at Santiaguito is shown in Figure 6. Explosion 6a in is an example of a weak plume which maintained a small initial diameter (~50m) throughout its duration, probably being constrained to the inner annulus. The explosion began with a small, grey, ash-rich head, seen in a.i, and lasted nearly 5 minutes, emitting a constant gas stem (a.iii-a.iv). Example 6b begins with an initial small, weak pulse (b.i) and 15 seconds later two pulses are visible in b.ii. The contrast in opacity, highlighted by the red dotted line, distinguishes the visible boundary between the two pulses. A third pulse is visible at the vent in b.iii, 80 seconds after the initiation of the explosion, outlined by the red dotted line. It is darker in color than the stem of the previously emitted pulse. Example 6c begins impulsively and with a larger initial diameter (>100m) (c.i) than the previous examples. It was apparently richer in ash and had a well-defined spherical body at its head and a stem that connects it to the vent (c.ii). After about 1 min a prominent stem of ash and gas (~140m in diameter) is seen connecting the spherical head to the vent (c.iii), which rises buoyantly, though with less ash, for at least another 30 seconds. Explosion 6d is an impulsive and short-lived ash-rich explosion. After approximately 40 seconds the rising body completely detaches from the vent. In Figure 6d.iii a vortex is seen at the bottom of this body where atmospheric air is entrained. A continuous release of gas was present prior to and

throughout this explosion. This is seen in d.i-iv as the weak, white plume rising out of the east side of the vent.

Explosions were not separated into categories because there was no clear boundary between explosion styles. The examples in Figure 6 represent a continuous spectrum of activity. There were many explosions that fell between these examples in ash and gas content, initial diameter, and duration. Most of the explosions observed during this study were similar to the examples seen in Figure 6, 'a' and 'b', and a few were similar to 'c'. Example 'd' was a unique explosion.

Velocity and Height Measurements through Time

Observed velocities of the leading edge of explosions ranged from 3-22$m \cdot s^{-1}$ at heights of ~20-1900m above the vent. Typically, the first pulse had the lowest measured velocities closest to the vent and later pulses had higher measured velocities higher above the vent (Figure 7). Some late pulses were weaker and could be seen in cases when the wind had blown away obscuring lower clouds. Because of masking issues, it was not possible to directly measure near-vent velocities of most of the pulses that occurred after the first pulse. In a few instances pulses increased in velocity as they rose.

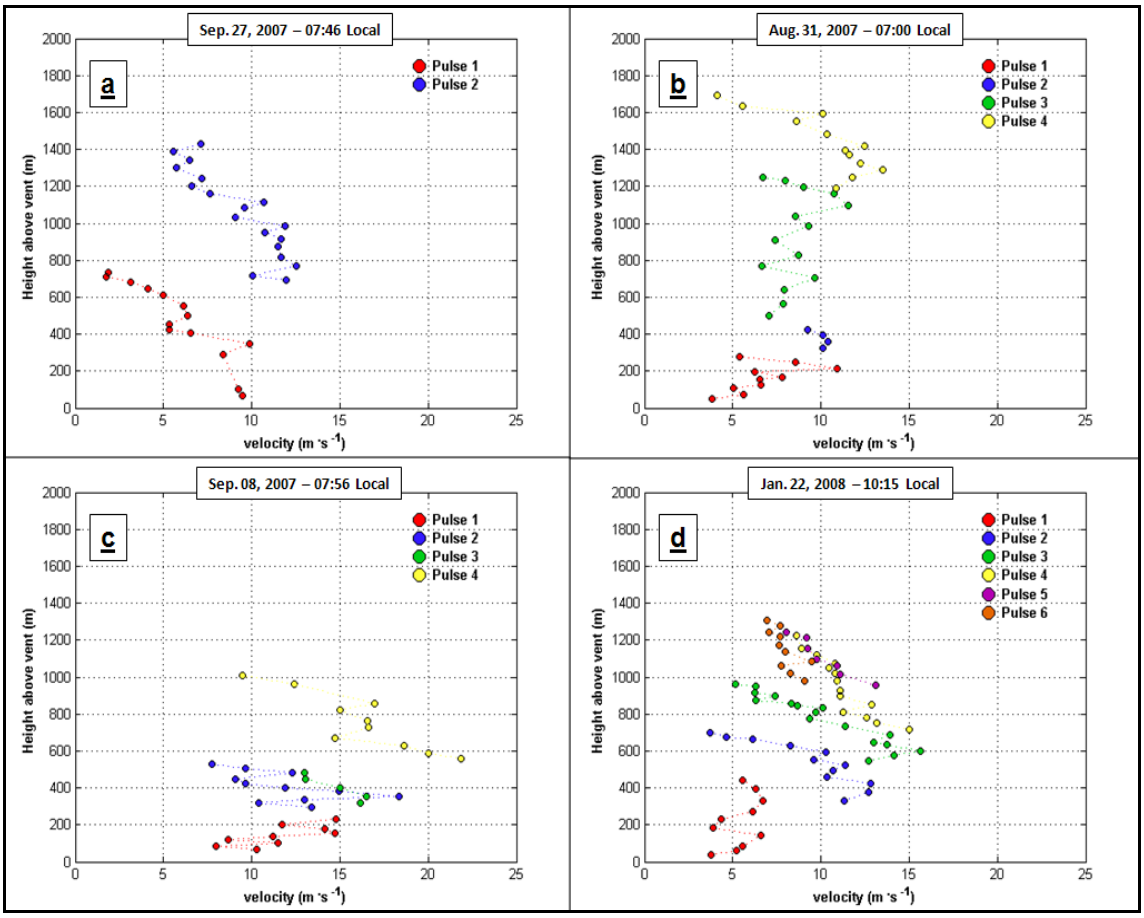

Figure 7. Velocity-height profiles of 4 distinct explosions with 2, 4 or 6 pulses, identified by color. Typically, where pulses could be identified, later pulses had higher velocities than earlier pulses at comparable elevations. Pulses were identified by the methods described above.

In order to estimate near-vent velocities, we used a 3rd degree polynomial fit of the height-time relations of the observed paths of the pulses. A 3rd degree polynomial is necessary because it accounts for changes in acceleration, which are observed in multiple pulses (Figure 8). A 2nd degree polynomial fit of the height time series is not adequate because it effectively produces a constant acceleration, which is not the case in all pulses. We extrapolated back in time until height was equal to zero and took the derivative to calculate the average velocity after one second (also referred to as the initial velocity). It is noted that these values do not truly represent the initial velocity as the ejecta leave through the fractures, but rather it is a measurement of the pulses that resulted from the combination of ash-laden jets, pressurized gas and ash, and weak

emissions of gas (Figure 5). Also, because we only see a pulse through part of its rise, we cannot capture its dynamics near the vent.

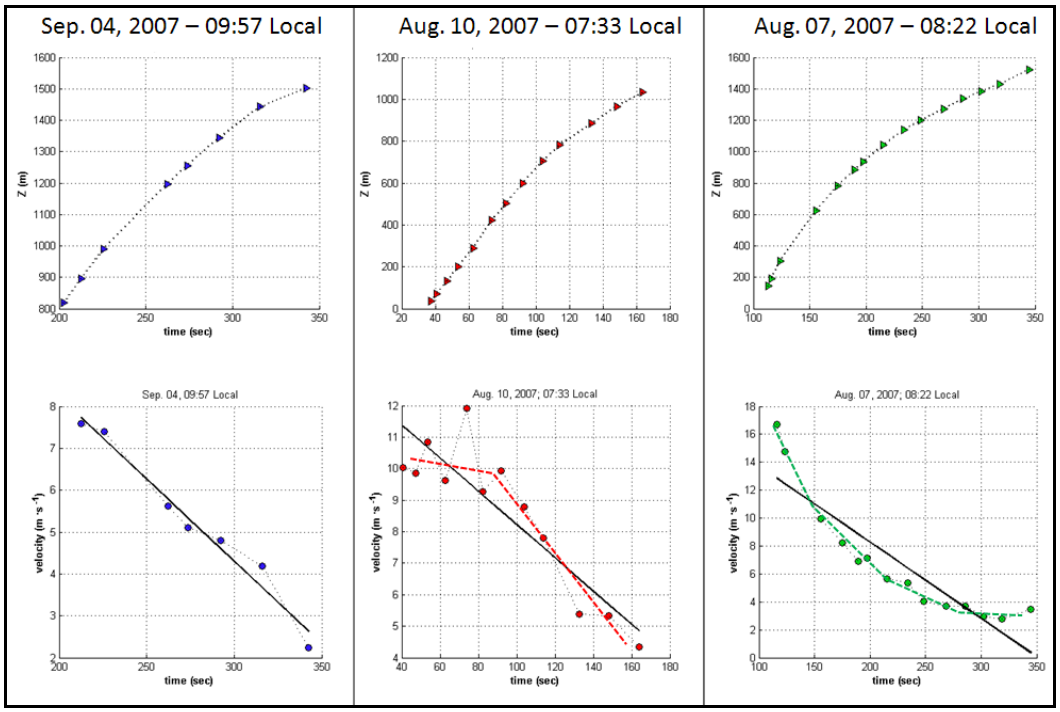

Figure 8. Plots of height (top) and velocity (bottom) over time for 3 separate pulses. **Left.** Constant acceleration, as velocity decreases at a constant rate. **Center.** Velocity decreases slowly then rapidly. The dashed red line represents 2 acceleration values, each defined by a unique slope. **Right.** Acceleration steadily changes. The dashed green line in the bottom right plot shows the acceleration is always changing. In the velocity plots the straight black line represents a 1st degree polynomial fit of the velocity over time, and represents a constant acceleration. The dashed lines have no mathematical value and are only included to emphasize the trends.

Initial velocities were on the order of ~0-35m s^{-1} (Figure 9, top left). On the right, a ratio of initial velocity of each pulse to the initial velocity of the first pulse shows that the first pulse did not always have the lowest velocity. With the exception of a few outliers, pulses typically had velocities up to three times the initial velocity of the first pulse in the same explosion (Figure 9, top right). If the initial velocity of the first pulse of a particular explosion is very low (~5m s^{-1}) and the later pulses have initial velocities of near 25-30m s^{-1}, then the ratios become very large. Average acceleration after 1 second was calculated to be -3-1m s^{-2} (Figure 9, bottom left). Most values range between -1-0 m s^{-2}. Pulses that had higher initial velocities also decelerated more quickly (Figure 9, bottom right). This pattern was not dependent on the pulse number.

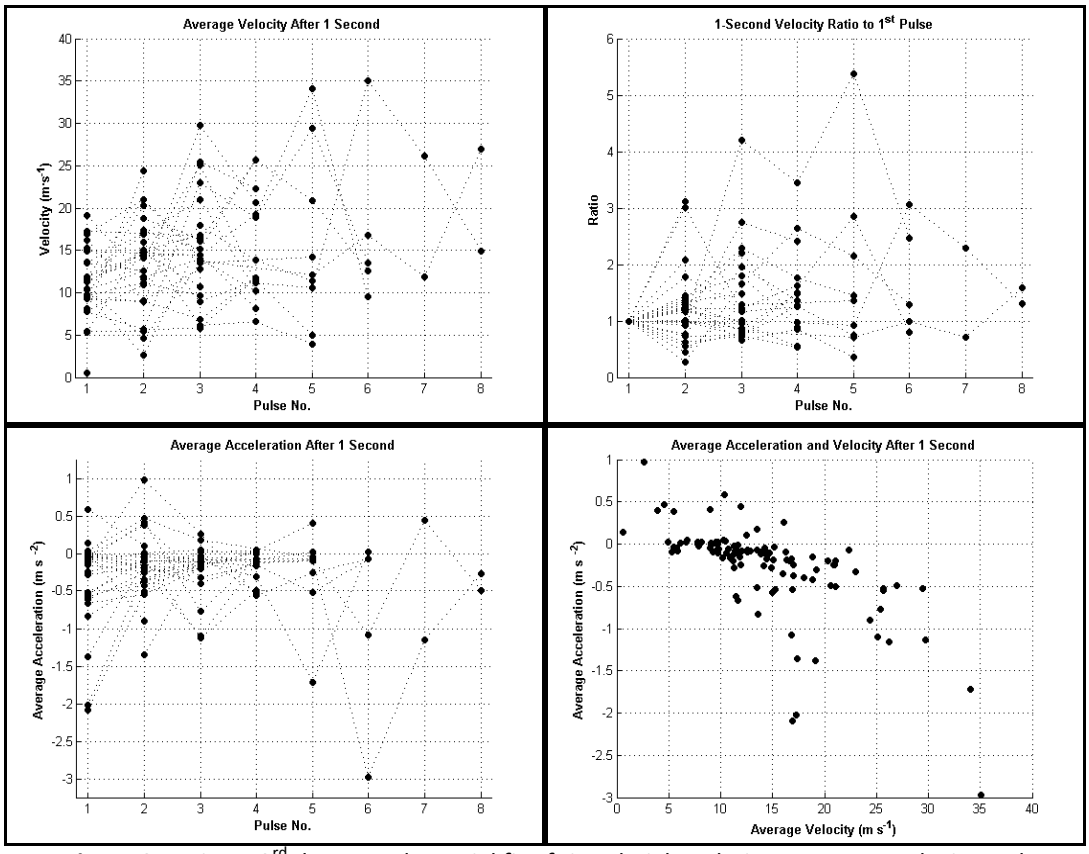

Figure 9. Using a 3rd degree polynomial fit of time-height relations, average velocity and acceleration are calculated after one second for each pulse. **Top Left.** Average velocity calculated after one second. **Top Right.** Ratio of 1-second velocity of each pulse divided by 1 second velocity of first pulse. In cases where values of greater than 35m s^{-1} were calculated, the points (12 in total) were discluded because there was a large gap between pulses that were measured at ~35m s^{-1} and the next highest velocity measurement. Pulses from the same explosion are connected by a dotted black line. **Bottom Left.** Average acceleration after one second. **Bottom Right.** Average velocity versus average acceleration after one second.

Measured velocities and measured heights for pulses 3 and 4 are nearly identical which is coincidental that the mean number of pulses per explosion was 3.8 (Mode = 4) (Figure 10). Maximum measured heights among pulses were typically ranged 400-1000m but do not represent the actual heights the pulse achieved. Some were measured up to 1900m. The highest measured pulse from each explosion was 650-1900m (average = 1125m). The average measured velocity values of all pulses were very similar (Pulses 1-6 average 10-13m s^{-1}) (Figure 10, left). This can be misleading because these velocities were measured at increasing heights (right). Because they are measured at higher

points they are affected more by deceleration as they rise, so they should have higher initial velocities.

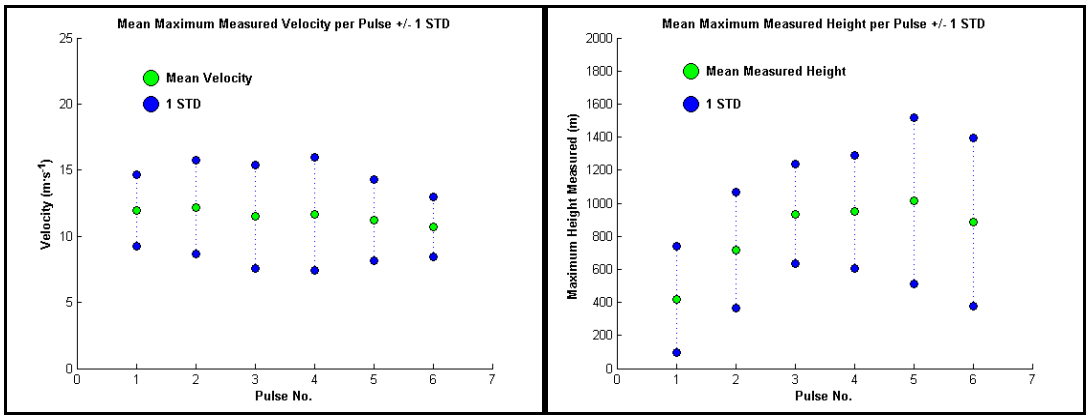

Figure 10. Velocity (**left**) and height (**right**) statistics for the first 6 pulses of observed explosions.

Constraining Flux Rates

Though we have observed pulsating explosions, they can still be considered as plumes since the pulses are closely spaced in time (Wilson, 1978). Sparks et al. (1997, pg. 118-120) present an empirically-derived relation that predicts the height of an eruption column based upon the eruption rate. Data was gathered from an extensive list of eruptions with recorded heights and eruption rates

$$H = (1.67) \times Q^{0.259} \qquad \text{(eqn. 1)}$$

where H is the height of the column in kilometers and Q is the volume eruption rate ($m^3 s^{-1}$). The correlation coefficient, R, equals 0.921, so available the data do follow the predicted trend. In this evaluation we use the average maximum explosion height which was about 1100m, or 1.1km (range 800-1800m). From equation 1, a value of $0.199 m^3 s^{-1}$ is derived for the volume flux of dacite magma. Using a density of dacite at Santiaguito of 2600 kg m^{-3} (Rose, personal communication, 2009), this corresponds to an average mass eruption rate of 517kg s^{-1} (range 130-3450 kg s^{-1}). The average duration of an explosion was about 180 seconds so the total erupted mass has a value of 9.3×10^4 kg (range = 2.3×10^4 - 6.2×10^5 kg). Yamamoto et al. (2008) calculated that one explosion may have contained as much as 2×10^4 metric tons (2×10^7 kg) of ash, but

this estimate is much higher than what was typical during the study periods described here.

Morton, Taylor, and Turner (1956) modeled the height of gas plumes from smoke stacks and estimated the height of a plume as a function of the thermal flux and thermal structure of the atmosphere. Adapted by Settle (1978) this relation is written as:

$$H = 7.89\,(1+\eta)^{-3/8} Q_H^{1/4} \qquad \text{(eqn. 2)}$$

where η is the environmental lapse rate (~-6.5˚C km^{-1}) divided by the adiabatic lapse rate (9.8˚C km^{-1}) (Wilson et al., 1978) and Q_H is the thermal flux (cal s^{-1}). Crosswind conditions are ignored in this analysis.

To calculate the heat energy from ash, we used a specific heat value for dacite of 0.2747cal g^{-1} ˚C^{-1} from Zellmer and Clavero (2006), taken from Bacon (1977). Grain size of the ash in these explosions is much smaller than 1mm (Rose, Unpublished, 2009). Small particles are more efficient in transferring their heat to colder air. If we assume a heat transfer efficiency of 0.9, because of the small size of the particles, a total of 1.34 x 10^{10} calories from ash contribute to the total thermal flux.

Dalton (personal communication, 2009) estimated the sulfur dioxide (SO_2) flux during an explosive event reached 1.4kg s^{-1}, and between explosions is much lower, around 0.2kg s^{-1}. We can estimate the total SO_2 mass for an explosion, including several pulses, which last a total of ~3 minutes on average by multiplying 1.2 kg·s^{-1} (1.4-0.2) times 180 seconds to get 216 kg SO_2. The H_2O mass can be expected to be about 100 times the SO_2 mass if we look at typical well sampled andesitic and dacitic volcanic gases (Symonds et al., 1994, Table 3), so this corresponds to about 2.16 x 10^4 kg of H_2O. If we assume that a) all the gas released is H_2O (The real proportions are 90-95% H_2O), b) the temperature of that gas is the same as the Santiaguito magma (850˚C, Harris et al. 2002, Table 2) and c) cools to a local temperature of 10˚C, we calculate that about 2.98 x 10^{10} calories are released by the gas alone as it cools and condensates. This is more than double the amount of calories released by ash, and is contrary to typical results which suggest that

the majority of thermal energy should come from pyroclastic material produced by an explosive eruption (Settle, 1978). A total thermal flux of 2.4 x 10^8 cal s^{-1} is obtained from ash and gas. In a stable environment, where crosswind conditions can be neglected, the calculated height from equation 2 is 1,445m. This result is reasonable considering that if we included crosswind effects, the upward movement of the plume would be inhibited (Settle, 1978).

An important parameter of volcanic explosion clouds is the gas mass fraction, n, defined as the mass of the gas content divided by the sum of the mass of erupted gas and lava.

$$n = m_{gas} / (m_{gas} + m_{lava}) \qquad \text{(eqn. 3)}$$

Patrick (2007a) describes the effects of the relation between initial plume bulk density and n_{plume}, which discludes particles that rapidly decouple from the gas phase. n_{plume} is relatively small (<0.05) for plinian eruptions, which depend on entrainment and heating of atmospheric air to become buoyant. Gas mass fraction values that exceed gas contents found in magmas indicate that gas has decoupled from the magma and has concentrated prior to eruption, as was the case in Strombolian eruptions at Stromboli Volcano (Patrick, 2007a). Patrick calculates for magmatic and gas temperatures of 800˚C (about 50˚C less than Santiaguito), the gas mass fraction of plume only needs to be 0.17 to be initially buoyant and 0.28 if ash is at 20˚C. These limits increase for higher temperatures. Since we know the mass of the gas and lava that are erupted during a typical event we can calculate the plume gas mass fraction (n_{plume}), which according to equation 3 is 0.19. Plumes that only rose to heights of about 800m had higher gas mass fractions (0.48) due to less ash present in the plume.

Discussion

Explosion Characteristics

Explosions at Santiaguito can best be described as explosive emissions of varying amounts of gas and ash that develop into 1-8 main pulses within the resulting plume (mode = 4 pulses per event; std. = 1.5). Individual explosions last 30-300 seconds and

typically reach heights of 700-1500m above the vent. Explosions typically begin with a weak initial pulse that is followed by stronger pulses, and may conclude with another weak pulse. Sahetapy-Engel et al. (2008) also observed a weak initial gas puff with a thermal sensor, which preceded the main emission. In a later field campaign, this was observed with a FLIR camera from the summit of Santa Maria (Sahetapy-Engel et al., 2009); an initial, weak emission from near the center of the vent, followed by stronger emissions through a series of fractures surrounding the initial emission. The later emission developed into a pulse which overtook the previous. Observations from the summit of Santa Maria indicate that these initiations occur from along an inner ring fracture, an outer ring fracture which is the boundary of the entire vent, or smaller fractures between the two ring fractures.

An average explosion (height = 1100m, duration = 180s) contains on the order of 93 metric tons of ash and 31 tons of gas, mainly water vapor. The result is a high gas mass fraction (0.19). This value falls above the minimum limit (0.17) required for a plume to be initially buoyant as described by Patrick (2007a).

Plume Morphology

Volcanic cloud forms observed at Santiaguito, as described by Morton et al. (1956) and Turner (1962; 1973), include plumes, starting plumes, and one discrete thermal (all seen in Figure 6, a.ii-iv, c.ii, and d.ii-iii, respectively). Patrick (2007) observed another type of morphology at Stromboli volcano which was also observed at Santiaguito during this study; a rooted thermal, which is described as a combination of a starting plume and a discrete thermal in that it has a stem between the rising head and the vent, but also has a noticeable vortex ring at the base of the rising front (Figure 11). Scorer (1957) concluded that all significant air entrainment occurs at the base of the rising body, so the absence or presence and magnitude of this stem plays a major role in plume dynamics, affecting rise height, velocity and lateral spreading rates. If the head of the rising plume only incorporates gas and ash from its stem it will receive extra energy

supplied as buoyancy, and will be able to rise faster and higher. The plume will not expand much because the entrained fluid is already as hot as the leading head. The absence of the stem causes the entrained fluid into the rising thermal to be colder and denser. In this case the excess heat is finite and the cold air will be heated causing it to expand. A gaseous stem indicates that either 1.) ash has been emptied from within the fractures and there is still a supply of gas within the system or 2.) there is not a high enough exit velocity of gas to support ash. The presence of a stem indicates that the fractures within the vent do not reseal rapidly.

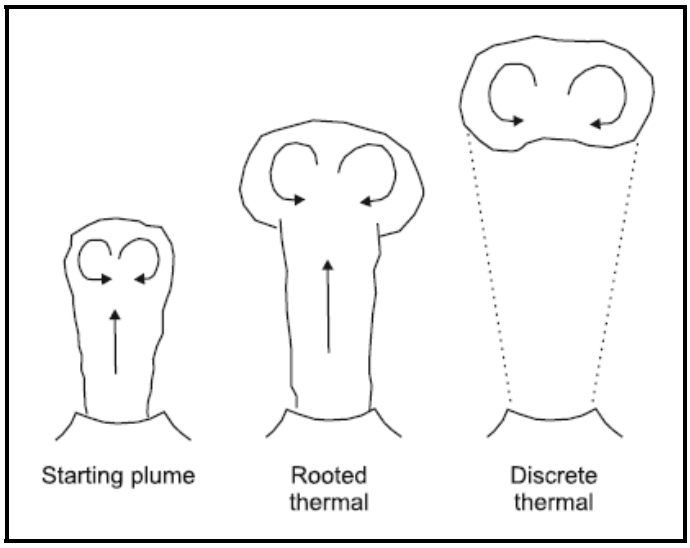

Figure 11. Showing observed cloud morphologies. From Patrick (2007) with permission (See Appendix II).

Relationship between Plumes and Conduit

It has been suggested that extrusion through the conduit mainly occurs during explosions in sudden movements of the plug (Bluth and Rose, 2004; Sahetapy-Engel et al., 2008; Johnson et al., 2008). The pulsating behavior of the plumes we observed is evidence that this movement may be unsteady and not evenly distributed throughout any explosion. Bluth and Rose (2004) first suggested that in each explosion the plug will slip once, and evidence of the possibility of multiple slips in a single explosion was first inferred by Sahetapy-Engel et al. (2008). We were unable to correlate the degree of movement in each slip to the velocity and size of each pulse and explosion, though Bluth

and Rose (2004, Figure 2) estimate that the plug may move up to ~0.1m per explosion (estimating a conduit diameter of 50m).

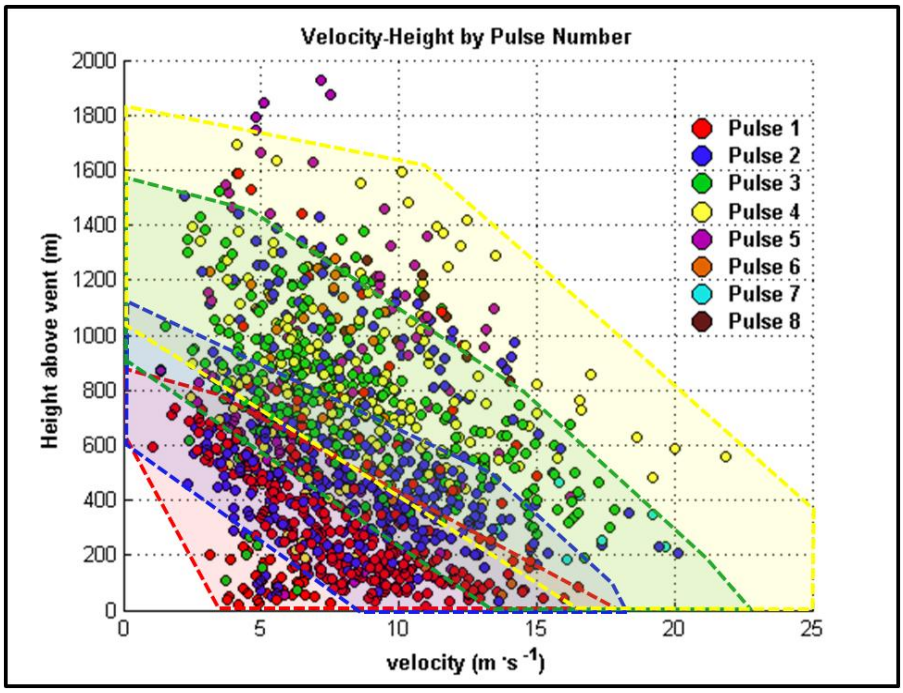

Figure 12. Cloud top velocity versus height for individual pulses with the pulse number identified by color. Data for all studied explosions are included. Shaded regions outlined by dashed lines represent typical velocity values for each and projected range of velocities at lower heights for the first 4 pulses (red blue, green and yellow). These tend to go progressively higher as also shown in Figure 10 (right).

Figure 12 is a compilation of all explosions analyzed in this study, similar to Figure 7. Typical height-velocity points for the first 4 pulses are outlined by dashed lines (line colors correlate to key, described in figure text). The initial pulse of each explosion typically has the slowest rise velocities and higher velocities were measured for subsequent pulses at comparable heights above the vent. This suggests that as an explosion progresses later pulses have higher initial velocities than the initial pulse. The magnitude of the velocity may be proportional to how much the plug slips during each pulse. As shown in Figure 9, however, this may not always be the case, suggesting it is reasonable that later pulses could have lower initial velocities.

Because explosions discharge material through a series of fractures and last on the order of minutes, it is reasonable that the gas that drives the explosions is stored vertically within the the plug-conduit wall boundary and within other minor fractures beneath the surface. This would explain why the explosions last nearly 3 minutes on average; it would require more time for gas to be expelled from a long and deep source rather than from a large source near the surface.

At the onset of an explosion gas is released from within annular fractures that outline the conduit and a series of smaller fractures within the vent. Gas within the fractures near the surface is under the least amount of pressure and therefore does not exit at high velocities. Because of the proximity to the surface, gas within these fractures may also leak out more easily. As an explosion progresses, gas from deeper within the system makes its way towards the surface. Because it was under higher pressure and little gas has escaped, it exits at a higher velocity and carries more ash. Throughout an explosion the network of fractures opens as gas passes through causing the activity at the vent to propagate outwards towards the edge of the vent. The supply of gas with in the system eventually is depleted and the gas that is emitted does so with less force than previously; it carries less ash and is immediately sucked horizontally towards the base of the plume.

The network of fractures in the system is variable and the gas stored within these fractures is unevenly distributed. This is demonstrated by certain parts of the annular fractures opening at different times with different intensities and discharging variable amounts of ash (Figure 5). The degree to which these fractures are opened may vary in each explosion and therefore when the explosion subsides the fractures may not reseal to how they were before the explosion. This creates an ever-changing network of fractures at the vent.

Similarities to Short Explosions at Other Volcanoes

Small ash-rich basaltic explosions were observed at Fuego Volcano, also in Guatemala, in 1978 (Wilson & Self, 1980). They were described as vulcanian explosions, producing "discrete, uniformly grey and apparently homogenous cloud(s) and released gas and particles." Initial velocities were of a similar in magnitude (5-30m s^{-1}) to those at Santiaguito during this study. Though these explosions apparently consisted of a single pulse, their form was similar to explosions at Santiaguito, being either cylindrical or spherical in shape.

Patrick et al. (2007b) described the dynamics of small, basaltic, strombolian explosions in detail at Stromboli volcano. Three types of explosions were described. Type 2a and 2b explosions are the most similar in that they consisted of a low to high contents of ash and displayed momentum and buoyancy driven regimes. Visible plumes and thermals with radii of up to 35m were identified. Explosions were interpreted to have resulted from the bursting of over-pressurized slugs.

The 1997 Montserrat explosions (Formenti et al. 2003) began with ballistic ejections followed by fountain collapse (forming pyroclastic flows) and concluded with the formation of a volcanic plume which detached and rose as a thermal to 3-15km. These explosions were termed vulcanian and each erupted ~3 x 10^5 m^3 of andesitic magma. Explosions were described to have happened due to rapid fragmentation in the conduit, which was drained 1-2km during each explosion.

Table 2. Summary of other volcanoes with similar explosion clouds.

Volcano	Observation Period	Eruption Mechanism	Explosion Description	Explosion Velocities
Santiaguito	Jul. 2007 - Mar. 2008 (descriptions similar since 1968)	Plug Stick-slip	Continuous pulsating emissions of ash and gas through fractures in the vent producing sustained plumes	5-45m s^{-1}
Montserrat (Formenti et al., 2003)	Oct. 1997	Rapid fragmentation	Sequence of ballistics, fountain collapse producing pyroclastic flows, then generation of buoyant plume and thermal	40-100^{+} m s^{-1}
Stromboli (Patrick, 2007)	Jun. - Jul. 2004	Over-pressurized gas slug	Plumes and thermals with low to high ash contents and buoyant and momentum driven rise regimes	5-45m s^{-1}
Fuego (Wilson & Self, 1978)	Nov. 1978	Not described	Ash-rich basaltic explosions with uniform cylindrical and spherical clouds of gas and particles	5-30m s^{-1}

These descriptions raise the question of how to term an explosion or eruption; should classification come as a product of the resulting volcanic clouds or the eruption mechanism? We have described how four different volcanoes (3 mechanisms described) produce similar explosion clouds of varying intensity. It seems reasonable that the terminology should be a product of the resulting volcanic clouds rather than the eruption mechanism. Morrissey and Mastin (2000) also describe vulcanian explosions as short lived (seconds to minutes) explosions that may pulsate and expel material that is typically of higher silicate content (andesitic basalt-dacite). By this methodology, Santiaguito explosions most resemble low-intensity, vulcanian style explosions.

Conclusions

Characteristic explosions at Santiaguito during July 2007 - March 2008 are continuous, pulsating releases of hot ash and gas erupted unevenly through a system of fractures in and around a dacite plug. Volcanic clouds, typically in the form of plumes, rise to heights of 650-1900m above the vent. Explosions typically occurred every 15-150 minutes and lasted on average about 3 minutes (30 seconds – 5 minutes). Using the

model from Sparks et al. (1997), we calculated that the mass eruption rate is on the order of 517kg s^{-1} (range = 130-3450 kg s^{-1}). Using a 3rd degree polynomial fit of the height-time relations, initial velocities of the pulses are around 5-45m s^{-1}. These values are comparable to velocities at other volcanoes (Fuego and Stromboli) that display vulcanian and strombolian eruptive activity. High gas mass fractions values (>0.19) suggest that plumes may be initially buoyant.

The pulsating nature observed in the plumes can be interpreted to represent multiple slips of the dacite plug. Typically, the first pulse is the weakest and is soon overtaken by later pulses that have higher initial velocities and larger widths at their base. The increase in initial diameter (as seen from OVSAN) is representative of the propagation of emissions from the inner annulus towards the outer limits of the vent (sometimes seen from the summit of Santa Maria). Some explosions are confined to the inner annulus (not within it), while larger explosions may start around the inner annulus and eventually reach the outer annulus as they propagate outwards through minor fractures.

Explosions can be referred to as weak vulcanian style eruptions due to their duration (seconds to minutes), pulsatory nature, and high-silicate ash content (Morrissey and Mastin, 2000). They are also similar to other observed volcanic clouds that were described as vulcanian at Fuego in 1978 and Soufriere Hills in 1997.

It is unclear what effect pulses have on each other during a single explosion. On one hand, a pulse that follows in the path of a previous pulse will entrain warmer air and material, which will contribute to its overall buoyancy. On the other hand, there is a smaller temperature and density difference between the stem of a leading pulse and the head of a following pulse, which has a negative effect on the buoyancy of the later pulse. Further investigation is also necessary to detail how smaller scale events that take place at the vent contribute to the variable morphology of the resulting volcanic

clouds. Over longer time periods (10's of years) it would be beneficial to compare cloud morphology to the type and level of activity (lava flows, extrusion rate, and likelihood of pyroclastic flows) because the explosion clouds are the most visible sign of volcanic activity to the surrounding communities.

Acknowledgements

Financial Support for this research came from The US National Science Foundation through grants EAR 0451447 and PIRE 0530109, from the US Peace Corps and from teaching assistantships at Michigan Tech's Department of Mining and Geological Engineering & Sciences. Thanks are owed to many people, especially my advisor, William Rose, for making this opportunity possible. For helping me form my thesis and put it together, my other committee members, Greg Waite, Jose Luis Palma, and Sandra Boschetto-Sandoval. Matt Patrick provided me with ideas from abroad. Flavio Linares and Eddy Sanchez for creating a link between INSIVUMEH and the Peace Corps and being so enthusiastic about the Master International program. La mara at INSIVUMEH including, Gustavo Chigna, Otoniel Matias, Julio Cornejo and Alvaro Rojas were all helpful professionally as well as were exceptional friends. The people of El Faro, Patzulin, La Florida and Las Marias for welcoming me into their communities. An internship visit from Edrick Ramos at The University of Puerto Rico at Mayaguez was vital in establishing the video analysis system used in this study. John Lyons and Rudiger Escobar-Wolf have provided me with key insights to Guatemalan volcanology and have caused me to think critically about my research. And of course thanks to all of my family and friends for supporting me through Peace Corps and my research that followed.

References

Agrawal , A., and A.K. Prasad (2003), Integral solution for the mean flow profiles of turbulent jets, plumes and wakes, *J. Fluid Eng*., 125, 813-822.

Bacon, C.R., (1977), High temperature heat content and heat capacity of silicate glasses: Experimental determination and a model for calculation, *American Journal of Science* 277, 109–135.

Bluth, G.J.S., W.I. Rose, (2004), Observations of eruptive activity at Santiaguito Volcano, Guatemala. J. Volcanol. Geotherm. Res., 136, 297-302.

Bowman, L., L. Kapelanczyk, A. Colvin, O. Matías, W.I. Rose, M. Rios-Sánchez, R. Escobar-Wolf (2008), Estimating Thermal Energy Emission and Eruption Rates at Guatemalan Volcanoes Using Thermal Data From a FLIR Camera, ASTER, and MODIS Data Sources, American Geophysical Union Fall 2008 Meeting Poster.

Branan, Y.K., (2007), Investigating Short-Term Variation in Volcanic Plume and Shallow Subsurface Dynamics Using High Temporal Resolution Gas Emission Rate Data. Ph.D. Thesis, Michigan Technological University.

Brown, D. (2008), http://www.cabrillo.edu/~dbrown/tracker/.

Durst, K.S. et al., (in Review), Erupted Magma Volume Estimates at Santiaguito and Pacaya Volcanoes, Guatemala using Digital Elevation Models.

Harris, A., W.I. Rose, L.P. Flynn (2003) Temporal trends in lava dome extrusion at Santiaguito 1922-2000, *Bull Volcanol.*, 65: 77-89. DOI: 10.1007/s00445-002-0243-0.

Escobar-Wolf, R.P. O. Matias, W.I. Rose., Santiaguito Dome Geologic Map, 2008.

Escobar-Wolf, R.P., J.F. Diehl, B.S. Singer, W.I. Rose, (in Press), $^{40}Ar/^{39}Ar$ and paleomagnetic constraints on the evolution of Volcan de Santa Maria, Guatemala.

Formenti, Y., T.H. Druitt, K. Kelfoun, (2003), Characterisation of the 1997 Vulcanian explosions of Soufriere Hills Volcano, Montserrat, by video analysis, *Bull Volcanol.*, 65: 587-605. DOI: 10.1007/s00445-003-0288-8.

Johnson, J.B., A.J.L. Harris, S.T.M. Sahetapy-Engel, R. Wolf, W.I. Rose (2004), Explosion dynamics of pyroclastic eruptions at Santiaguito Volcano, *Geophys. Res. Let*., 31, L06610. DOI: 10.1029/2003GL019079.

Johnson, J.B., J.M. Lees, A. Gerst, D. Sahagian, N. Varley (2008), Long-period earthquakes and co-eruptive dome inflation seen with particle image velocimetry, *Nature*, 456, 377-381.

Morrissey, M.M., and L.G. Mastin, (2000), Vulcanian Eruptions, Encyclopedia of Volcanoes, Academic Press, 463-475.

Morton, B.R., Sir Geoffrey Taylor, J.S. Turner, (1956), Turbulent gravitational convection from maintained and instantaneous sources, *Philosophical Transactions of the Royal Society London A*, v.234, 1-23.

Patrick, M.R. (2007), Dynamics of Strombolian ash plumes from thermal video: Motion, morphology, and air entrainment, J. Geophys. Res., 112, B06202, DOI:10.1029/2006JB004436.

Patrick, M.R. (2007a), The gas content and buoyancy of strombolian ash plumes, *J. Volcanol. Geotherm. Res*., 116 1-6.

Patrick, M., A.J.L. Harris, M. Ripepe, J. Dehn, D.A. Rothery, S. Calvari, (2007b), Strombolian explosive styles and source conditions: insights from thermal (FLIR) video, *Bull. Volcanol.,* 69, 769-784, DOI: 10.1007/s00445-006-0107-0.

Rose, W.I., R.E. Stoiber, S.B. Bonis (1970), Volcanic activity at Santiaguito Volcano, Guatemala June 1968 – August 1969, *Bull. Volcanol.*, *34*, 295-307.

Rose, W.I., (1973), Pattern and mechanism of volcanic activity at the Santiaguito volcanic dome, Guatemala, *Bull. Volc.*, 37, 73, 1973.

Rose, W.I., (1987) Volcanic activity at Santiaguito volcano, 1976 – 1984, *Geo. Soc. Amer. Spec. Pap.*, 212, 17-27.

Sahetapy-Engel, S.T., A.J.L. Harris, E. Marchetti (2008), Thermal, seismic and infrasound observations of persistent explosive activity and conduit dynamics at Santiaguito lava dome, Guatemala, *J. Volcanol. Geotherm. Res*., 173,1-14.

Sahetapy-Engel, S.T., A.J.L. Harris (2009), Thermal structure and heat loss at the summit crater of an active lava dome, *Bull. Volcanol.*, 71, 15-28.

Settle, M., Volcanic eruption clouds and the thermal power output of explosive eruptions, *J. Volcanol. Geotherm. Res.,* 3, 309-324.

Scorer, R.S., (1957), Experiments on convection of isolated masses of buoyant fluid, *J. Fluid Mech*., 2, 583-594.

Sparks, R.S.J., M.I. Bursik, S.N. Carey, J.S. Gilbert, L.S. Glaze, H. Sigurdsson, A.W. Woods, (1997), Volcanic Plumes, Wiley, Chichester.

Terada, A., Y. Ida, Kinematic features of isolated volcanic clouds revealed by video records, *Geophys. Res. Let.*, 34, L01305, DOI: :10.1029/2006GL026827.

Turner, J.S. (1962), The starting plume in neutral surroundings, *J. Fluid Mech*., 13, 356-368.

Turner, J.S. (1962b), Model experiments relating to thermals with increasing buoyancy, *Quarterly Journal of the Royal Meteorological Society*, 82, 62-74.

Turner, J.S. (1969), Buoyant plumes and thermals, Annu. Rev. Fluid Mech., 1, 29-44.

Turner, J.S. (1973), Buoyancy Effects in Fluids, Cambridge Univ. Press, Cambridge, UK.

Williams, S.N., S. Self, (1980), Volcanic Explosion Clouds: Density, Temperature and Particle Content Estimates from Cloud Motion, *J. Geophys. Res.*, 85, 2567-2572.

Williams, S.N., S. Self, (1983), The October 1902 Plinian eruption of Santa Maria Volcano, Guatemala, *J. Volcanol. Geotherm. Res*., 16, 33-56.

Yokoyama, I., (1957), Energetics in active volcanoes, *Bull. Earth. Res. Inst.*, 35, 75-97.

Yamamoto, H., I.M. Watson, J.C. Phillips, G.J. Bluth (2008), Rise dynamics and relative ash distribution in vulcanian eruption plumes at Santiaguito Volcano, Guatemala, revealed using an ultraviolet imaging camera, *Geophys. Res. Let.,* 35, L08314, DOI: 10.1029/2007GL032008.

Zellmer, G.F., J.E. Clavero, (2006), Using trace element correlation patterns to decipher a sanidine crystal growth chronology: An example from Taapaca volcano, Central Andes, *J. Volcanol. Geotherm. Res., 156, 291-301.* DOI: 10.1016/j.jvolgeores.2006.03.004

Appendix I

Scaling

Explosions with minor lateral movement were analyzed until they reached a height above the crater where wind began to dominate the plume dispersion. We assume that explosions rise in a perfectly vertical direction because we cannot determine how much a plume may be tilted towards or away from our observation point. Horizontal plume dispersion is minimal because clouds are carried typically carried towards the west, which is horizontal to the perspective plane, meaning displacement towards or away from OVSAN is minimal. Since the elevations and distances are precisely known between OVSAN, the Caliente Vent and the Summit of Santa Maria, the video data can be geometrically corrected and accurately scaled. When the top of an explosion is in line with the Summit of Santa Maria the height above the vent is equivalent to 436m. Tracker inherently assumes that this 436m scale is valid at all heights, which is not true; due to the observation point being lower than the vent we always look up at the explosions. To correct for this, a secondary scale must be applied. For each degree increase in inclination, the rate altitude increases becomes larger, as well.

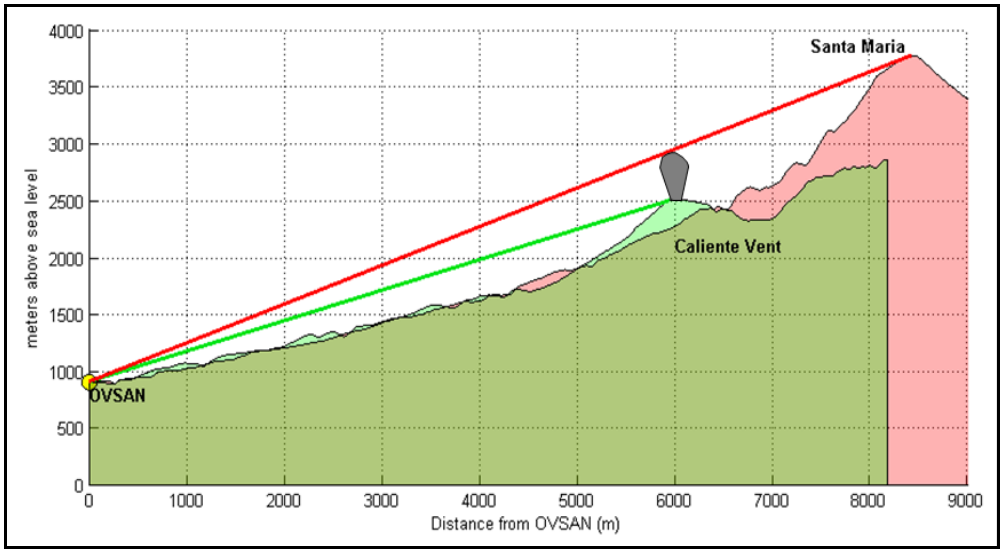

Figure 11. Scale 1. Cross sections of topographic profiles along the green and red lines in Figure X with a hypothetic explosion at a height of 436m.

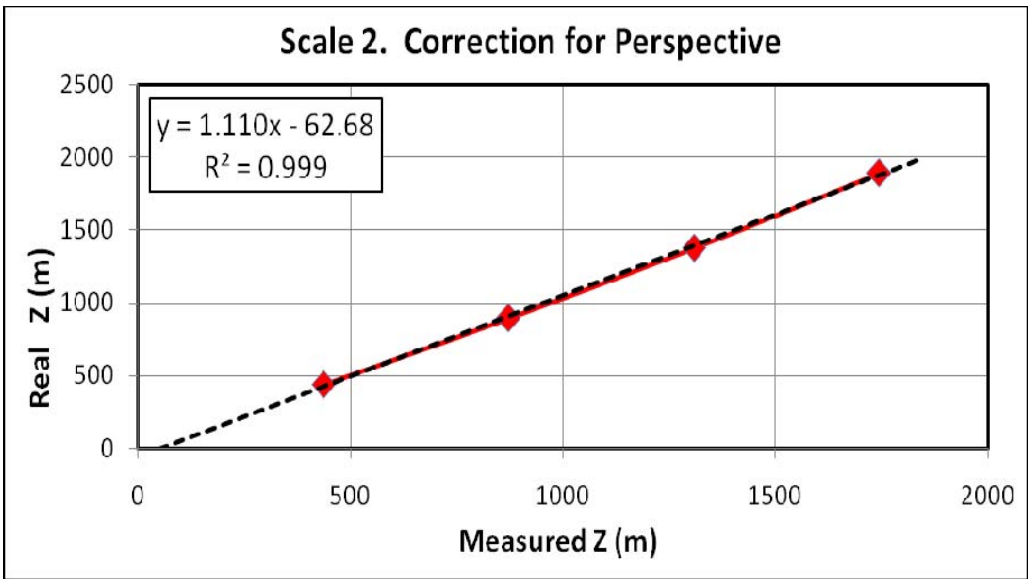

Figure 12. Scale 2. Appropriate scaling looking up towards rising volcanic clouds.

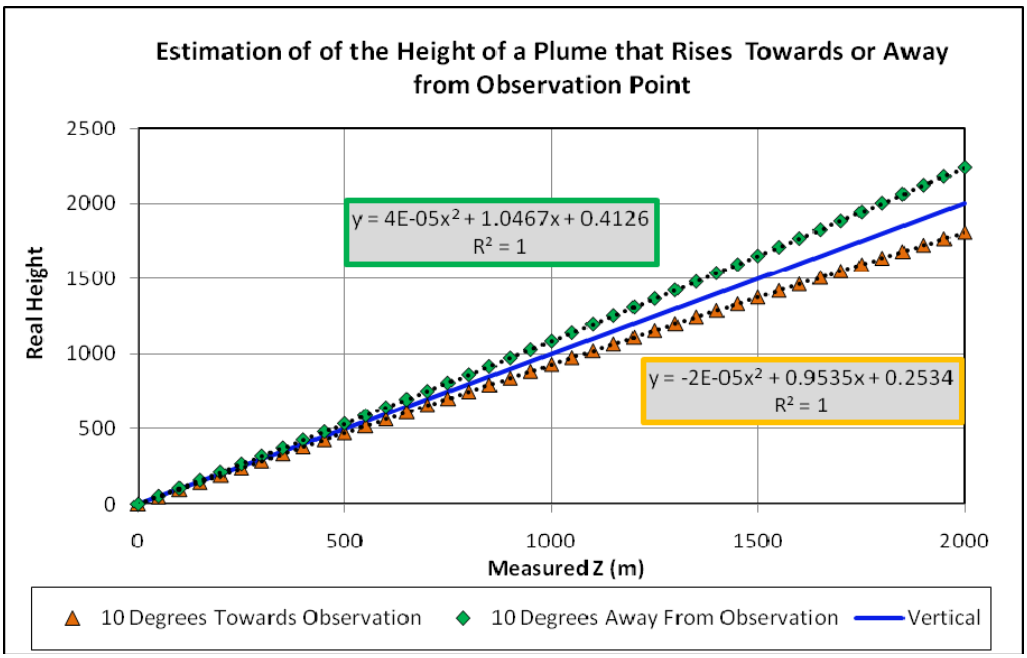

Figure 13. Scale 3. Appropriate scaling correction for a cloud that rise towards or away from the observation point

Appendix II

Email correspondence regarding permission to use figure

On 7/27/2009 1:11 PM, R Adam Blankenbicker wrote:
Good afternoon.

I am writing to request permission to use a figure in my Master's Thesis.

The figure of concern is from...

Patrick, M.R. (2007), Dynamics of Strombolian ash plumes from thermal video: Motion, morphology, and air entrainment, J. Geophys. Res., 112, B06202, DOI:10.1029/2006JB004436.
(Figure 2., pg 2 of 13.)

This figure was adapted (with permission) from Annual Review of Fluid Mechanics for the article...

Turner, J.S. (1969), Buoyant plumes and thermals, Annu. Rev. Fluid Mech., 1,29-44.

Please provide me the appropriate credit format you would prefer.

Thank you.
Best Regards.
-Adam Blankenbicker-

Response Received on July 28, 2009 3:16 PM
Mr. Blankenbicker,
That will be fine. Please use the format through the link provided below.

http://www.agu.org/pubs/citing.shtml

Thank you.

Brendan Tully
Editor's Assistant

Appendix III

Data from Tracker Video Analysis

July 01, 2007 - September 27, 2007			
		Video Time (sec)	Height After 436m Scale
7/1/2007	6:37:00 AM		
1		24.32	73.95
1		26.27	96.49
1		29.17	123.29
1		31.78	150.49
1		34.12	168.90
1		37.75	194.96
1		40.03	214.51
1		44.98	250.81
1		47.59	268.49
1		51.84	300.14
1		52.17	305.60
1		54.15	332.98
1		57.75	375.81
1		60.42	404.39
1		65.31	445.35
1		69.27	478.23
1		73.52	524.78
1		78.77	569.15
1		86.99	629.06
1		93.56	675.26
1		100.42	718.44
1		106.66	759.04
1		115.53	817.13
1		124.08	868.87
1		134.57	928.86
1		146.72	988.02
1		163.45	1057.83
1		182.16	1115.54
7/11/2007	7:55:00 AM		
2		191.57	30.28
2		192.46	41.37
2		196.98	85.74
2		199.65	113.47
2		203.25	147.86
2		208.69	175.59
2		216.74	201.10
2		220.34	258.68
2		223.94	304.26
2		228.43	356.40
2		232.02	391.89

January 22, 2008 - March 25, 2008			
		Video Time (sec)	Height After 436m Scale
1/22/2008	12:00:00 AM		
18		0.00	70.84
18		2.21	91.74
18		4.09	108.60
18		6.30	127.29
18		7.69	140.54
18		9.77	154.14
18		10.40	162.12
18		11.02	175.39
18		12.90	192.82
18		14.26	210.24
18		16.37	232.02
18		17.33	246.30
18		19.01	261.06
18		20.16	278.49
18		22.01	306.08
18		23.76	326.40
18		25.51	352.24
18		26.33	367.06
18		27.72	387.39
18		29.60	407.72
18		30.86	426.26
18		31.94	442.57
18		33.92	465.80
18		35.74	485.76
18		36.73	502.10
18		37.95	519.53
18		39.27	536.95
18		40.82	558.73
18		43.26	583.42
18		44.35	595.34
18		45.94	612.46
18		47.85	635.97
18		48.81	648.76
18		50.39	665.72
18		51.35	677.33
18		52.97	692.57
18		53.92	702.01
18		55.51	710.71
18		58.05	737.34
18		60.29	757.03

2		238.33	464.00
2		242.85	509.47
2		246.44	547.19
2		254.53	607.09
2		259.02	641.48
2		265.32	675.86
2		271.62	713.58
2			
2		231.13	225.51
2		242.85	367.49
2		256.31	521.68
2		260.83	574.92
2		276.11	716.90
2		281.49	760.17
2		289.61	825.61
2		294.99	864.43
2		302.18	921.01
2		309.38	958.72
2			
2		274.30	390.78
2		278.82	447.36
2		281.49	477.31
2		284.20	510.58
2		287.79	557.17
2		294.99	622.62
2		304.00	690.28
2		310.30	740.20
2		316.57	787.90
2		329.54	864.43
2		335.91	901.04
2		346.83	969.81
2		360.49	1045.24
2			
2		303.11	354.18
2		306.70	412.97
2		310.30	457.34
2		312.08	477.31
2		315.68	506.15
2		318.38	530.55
2		321.09	560.50
2		321.98	572.70
2		323.76	589.34
2		325.58	608.20
2		327.36	618.18
2			
2		324.69	256.92
2		335.94	356.81
2		340.46	401.20
2		345.91	454.47
2		352.28	516.62

18		62.21	772.39
18		64.45	789.61
18		66.66	803.60
18		68.57	818.03
18		70.82	827.54
1/22/2008	10:15:00 AM		
19		23.13	22.56
19		27.29	38.05
19		32.04	62.66
19		36.80	89.09
19		45.11	143.78
19		56.36	187.53
19		66.46	231.28
19		73.00	271.39
19		81.91	331.54
19		92.57	398.99
19		100.88	445.48
19			
19		86.39	269.56
19		92.17	335.19
19		95.67	379.85
19		99.13	424.51
19		102.63	460.97
19		106.10	498.34
19		108.41	524.77
19		111.90	558.50
19		115.96	600.42
19		120.02	634.15
19		125.80	669.69
19		128.14	680.63
19		134.51	704.33
19			
19		108.41	508.37
19		111.90	553.03
19		113.65	577.95
19		115.37	604.98
19		117.68	636.88
19		118.87	652.38
19		121.74	692.48
19		125.80	738.96
19		130.45	782.71
19		133.91	816.44
19		136.26	840.14
19		137.41	850.16
19		139.16	864.75
19		141.47	879.33
19		144.94	904.85
19		147.28	919.43
19		152.49	952.25
19		154.80	964.09

2		360.49	580.99
2		370.49	660.90
2		375.97	700.86
2		382.34	740.81
2		396.00	827.38
8/3/2007	8:30:00 AM		
3		58.74	45.28
3		62.34	91.36
3		68.34	139.29
3		75.54	187.21
3		82.73	246.19
3		86.33	268.31
3		89.93	290.43
3		94.71	318.07
3		111.47	423.13
3		115.07	454.47
3		121.08	509.76
3		124.67	546.63
3		133.06	609.29
3		140.25	649.84
3		145.07	690.39
3		153.45	736.47
3		169.03	810.20
3		176.22	841.53
3		184.60	872.87
3		194.21	906.04
3		206.18	944.75
3			
3		327.26	692.24
3		333.27	754.90
3		337.36	782.55
3		342.21	823.10
3		349.50	859.96
3		356.80	893.14
3		364.06	928.16
3		370.13	966.87
3		382.27	1012.95
3		396.83	1035.07
8/7/2007	8:22:17 AM		
4		52.44	55.19
4		54.32	86.08
4		56.23	108.15
4		60.06	147.87
4		62.90	165.52
4		65.77	195.31
4		69.60	229.52
4		75.31	279.17
4		81.02	334.34
4		84.84	370.75
4		92.47	433.64

19			
19		129.86	679.72
19		132.76	723.47
19		135.10	754.46
19		137.41	783.63
19		140.32	816.44
19		143.22	853.81
19		147.84	904.85
19		150.15	930.37
19		155.36	986.88
19		158.86	1024.25
19		161.77	1054.33
19		164.08	1078.94
19		168.73	1123.60
19		172.79	1159.15
19		180.87	1227.51
19			
19		164.08	932.19
19		166.39	962.27
19		171.60	1019.69
19		175.66	1063.44
19		179.72	1102.64
19		185.53	1155.50
19		191.90	1212.92
19		195.95	1244.82
19			
19		188.43	926.73
19		194.80	984.15
19		200.01	1026.99
19		205.23	1067.09
19		207.57	1088.96
19		213.94	1139.09
19		218.56	1173.73
19		224.96	1222.04
19		227.87	1242.09
19		232.49	1276.72
19		236.54	1304.07
1/29/2009	8:49:00 AM		
20		214.34	10.90
20		215.13	19.52
20		216.68	33.62
20		218.23	50.07
20		219.52	64.18
20		221.33	81.41
20		223.81	97.08
20		225.98	113.54
20		228.13	131.56
20		229.88	146.44
20		231.43	156.63
20		232.98	169.16

4		101.05	511.98
4		110.12	574.87
4		120.75	642.18
4		133.32	705.07
4		150.71	772.38
4		173.91	849.61
4			
4		113.03	144.86
4		115.93	193.44
4		123.65	307.86
4		155.53	627.83
4		174.87	787.36
4		189.35	887.13
4		197.08	941.91
4		215.42	1044.91
4		233.81	1142.01
4		248.29	1199.38
4		268.59	1272.20
4		285.98	1334.92
4		302.38	1381.44
4		318.81	1425.57
4		344.88	1511.55
4			
4		264.69	120.28
4		273.41	193.11
4		282.08	249.38
4		288.85	297.21
4		298.52	347.58
4		307.23	394.36
4		320.73	462.80
4		327.49	495.43
4		340.07	557.74
8/7/2007	9:28:27 AM		
5		58.58	31.74
5		62.44	57.12
5		67.58	104.71
5		75.31	159.71
5		79.83	194.61
5		84.35	227.39
5		91.41	278.16
5		97.81	317.29
5		109.53	402.95
5		116.72	451.60
5		129.10	504.48
5		140.18	544.67
5			
5		134.31	549.96
5		141.50	617.64
5		146.06	649.37
5		149.95	674.75

20		234.53	180.92
20		236.87	202.85
20		238.89	222.44
20		240.74	240.46
20		242.29	254.56
20		243.84	267.88
20		245.39	278.85
20		247.50	293.74
20		249.28	306.27
20		252.38	324.29
20		254.73	336.05
20		257.04	347.80
20		260.40	365.04
20		262.48	381.49
20		264.69	397.56
20		267.93	415.96
20		270.27	428.50
20		272.58	439.47
20		275.68	456.70
20		280.34	477.86
20		285.02	496.66
20		288.12	514.68
20		291.23	528.78
20		294.33	542.89
20		299.15	564.04
20		302.08	577.36
20		305.98	590.68
20		309.08	600.08
20		312.18	611.83
20		316.34	629.07
20		319.18	639.26
20		322.28	647.87
20		325.55	658.06
20		329.27	671.38
20		333.47	683.13
20		336.70	690.97
20		342.11	705.85
20		352.31	734.84
20			
20		241.30	128.42
20		243.51	146.44
20		244.96	159.76
20		246.44	172.30
20		248.66	190.32
20		252.32	216.17
20		256.01	240.46
20		258.23	253.00
20		259.68	263.18
20		263.37	279.64
20		266.31	291.39

5		151.93	698.02
5		156.49	733.98
5		162.36	776.28
5		166.91	803.78
5		170.18	822.82
5		174.74	857.72
5		181.93	908.48
5		185.82	930.69
5		192.98	960.30
5		200.84	993.09
5		208.00	1024.82
5		217.77	1061.83
5		226.25	1102.02
5		236.68	1155.96
5		249.08	1210.95
5		266.01	1273.35
5		290.80	1339.98
5			
5		161.04	638.29
5		166.25	664.18
5		171.47	694.85
5		176.68	722.35
5		179.32	738.21
5		181.27	755.13
5		186.48	798.49
5		193.64	839.74
5		200.18	883.10
8/9/2007	7:14:00 AM		
6		90.32	21.37
6		92.27	46.38
6		94.25	74.95
6		96.20	90.14
6		98.18	102.64
6		100.16	117.28
6		102.10	131.22
6		106.03	155.33
6		111.90	186.59
6		117.81	213.38
6		125.66	257.14
6		131.54	292.87
6		133.52	310.73
6		137.45	334.84
6		139.39	349.13
6		141.37	362.53
6		143.32	373.25
6		145.30	385.75
6			
6		141.37	333.06
6		143.32	354.49
6		147.25	387.54

20		268.19	307.06
20		269.68	315.68
20		271.46	325.08
20		274.40	336.83
20		276.61	347.02
20		279.54	360.33
20		282.48	372.09
20		283.24	379.14
20		285.42	392.46
20		287.63	408.91
20		291.32	426.15
20		294.99	441.03
20		297.92	451.22
20		301.62	459.84
20		303.83	475.51
20		306.77	491.18
20		311.19	509.98
20		314.13	522.52
20		318.55	538.19
20		321.49	552.29
20		325.15	568.74
20		331.06	586.76
20		338.02	607.92
20		349.17	642.39
1/29/2008	9:42:00 AM		
21		21.98	17.58
21		23.53	29.17
21		26.66	50.80
21		32.93	107.98
21		36.86	126.78
21		40.00	155.10
21		47.06	208.72
21		54.12	250.14
21		58.84	285.68
21		61.18	309.63
21		64.32	332.81
21		70.59	374.14
21		76.10	404.66
21		81.58	434.79
21		89.83	473.09
21		94.91	498.92
21		100.42	525.19
21		108.11	548.37
21		115.27	570.49
21		121.64	587.77
21			
21		29.04	29.94
21		32.93	50.80
21		35.31	63.94
21		37.65	75.53

6		151.21	415.22
6		157.05	454.52
6		162.95	488.45
6		168.83	517.03
6		172.76	531.32
6		173.22	533.57
6		178.79	572.87
6		188.10	630.05
6		197.44	680.07
6		208.59	731.89
6		219.78	772.98
6		230.93	819.43
6		245.85	881.96
6		255.16	905.19
6		275.65	957.00
6			
6		206.15	378.13
6		208.10	398.25
6		210.08	411.65
6		212.03	424.58
6		214.01	440.23
6		215.95	454.52
6		217.93	465.23
6		221.86	490.69
6		223.81	501.85
6		227.73	524.63
6		229.71	532.22
6		231.66	542.50
6		233.64	551.43
6		235.59	566.15
6		239.51	577.76
6		245.42	594.73
6			
6		221.33	458.09
6		225.29	485.57
6		229.22	510.36
6		237.14	552.04
6		241.10	574.57
6		243.08	585.84
6		247.37	598.31
6		251.30	624.20
6		257.20	649.21
6		259.15	659.93
6		261.13	667.57
6		267.00	691.19
6		270.93	707.26
6		274.86	727.80
6		278.78	746.56
6		284.69	762.26
6		288.62	782.28

21		40.00	88.66
21		42.37	100.25
21		44.72	111.84
21		47.85	128.06
21			
21		115.27	30.92
21		122.43	75.76
21		131.18	108.22
21		140.71	156.15
21		151.04	202.53
21		158.99	241.18
21		165.36	270.56
21		174.11	326.21
21		178.07	358.68
21		184.44	406.61
21		189.19	445.26
21		193.97	477.73
21		198.73	508.65
21		204.30	539.57
21		215.42	596.77
21		227.37	658.61
21		238.49	697.26
21		248.82	739.01
21		266.31	782.29
21		279.84	817.85
21		294.13	861.14
21		303.67	893.61
21		320.36	941.54
1/31/2009	8:12:00 AM		
22		26.37	14.41
22		27.79	33.62
22		29.70	57.49
22		31.61	82.31
22		34.95	115.72
22		38.81	152.96
22		41.71	180.65
22		48.05	237.93
22		52.40	275.16
22		57.26	323.85
22		65.01	384.00
22		80.06	490.93
22			
22		93.65	563.05
22		95.57	593.62
22		98.97	645.20
22		102.86	700.60
22		108.67	771.29
22		112.56	815.23
22		116.92	849.62
22		122.27	887.83

6		294.49	805.50
6		296.47	816.22
6		298.42	824.26
6		302.35	834.97
6		304.29	843.90
6		308.22	856.41
6		312.15	868.02
6		316.07	873.38
6		318.05	876.06
6		320.00	878.74
6		321.98	881.41
8/9/2007	7:53:23 AM		
7		62.17	238.48
7		72.96	302.26
7		81.31	357.18
7		89.50	406.79
7		102.86	472.34
7		116.00	520.17
7		124.38	546.75
7		135.14	583.95
7		148.30	598.12
7			
7		124.38	176.47
7		132.76	238.48
7		138.73	286.32
7		143.52	314.66
7		148.34	341.24
7		160.25	405.01
7		173.42	454.62
7		182.99	490.05
7		197.31	539.66
7		210.47	573.32
7			
7		192.59	327.06
7		198.53	383.76
7		206.88	456.39
7		214.07	497.14
7		218.86	523.71
7		226.02	553.83
7		238.00	598.12
7		247.57	621.15
7			
7		214.07	456.39
7		220.04	514.86
7		224.83	557.38
7		229.61	601.67
7		235.59	647.73
7		240.37	679.62
7		247.57	727.45
7		253.54	769.97

22		126.62	931.77
22		132.46	979.53
22		139.72	1029.20
22		146.52	1078.87
22		153.81	1124.72
22		159.16	1153.38
22		171.27	1201.14
22		182.92	1233.61
22			
22		131.51	782.12
22		135.86	809.81
22		138.77	836.54
22		144.61	880.46
22		148.47	904.32
22		150.41	921.51
22		153.81	953.01
22		158.17	988.34
22		161.07	1006.48
22		164.01	1028.44
22		168.37	1060.90
22		170.78	1082.86
22		174.17	1104.82
22		178.07	1130.59
22		186.32	1180.24
22		189.22	1205.06
22		192.62	1231.79
22		194.57	1244.20
22		196.98	1261.39
22		199.42	1281.44
22		202.32	1301.49
22		207.67	1342.54
22		211.07	1371.18
2/1/2008	8:09:00 AM		
23		140.84	111.77
23		152.66	204.76
23		166.65	272.26
23		174.04	310.48
23		185.82	384.35
23		193.22	446.77
23		204.27	520.64
23		209.42	560.13
23		214.60	591.97
23		224.93	653.11
23		238.19	718.07
23		246.31	757.56
2/26/2008	9:49:54 AM		
24		22.18	28.25
24		28.94	81.59
24		33.20	129.41
24		36.14	156.56

7		260.70	812.49
7		267.89	840.84
7			
7		330.03	89.66
7		334.95	148.13
7		342.34	222.54
7		350.96	298.72
7		358.35	358.95
7		366.96	433.36
7		381.74	544.97
7		394.05	621.15
7		410.06	679.62
7		417.45	718.59
7		434.71	764.66
8/10/2007	6:46:00 AM		
8		30.69	27.80
8		35.54	54.49
8		38.94	74.18
8		40.13	85.53
8		42.50	104.46
8		43.66	118.89
8		46.04	145.16
8		48.97	178.29
8		51.35	204.12
8		54.29	233.19
8		55.47	251.17
8		57.82	277.98
8		61.38	323.10
8		63.72	349.60
8		66.10	376.47
8		69.04	407.34
8		74.94	450.33
8		79.07	484.00
8		82.63	509.04
8		86.76	534.17
8		90.88	560.18
8		98.54	590.96
8		103.85	611.32
8		112.13	645.41
8		118.01	664.35
8			
8		67.85	312.07
8		73.16	367.00
8		76.73	410.56
8		80.26	452.23
8		87.35	520.41
8		92.07	575.33
8		95.60	605.64
8		102.70	649.20
8		106.82	677.61

24		41.51	209.90
24		45.41	240.48
24		52.24	294.24
24		57.12	337.49
24		60.06	358.76
24		69.83	415.34
24		76.66	456.43
24		79.60	471.27
24			
24		21.71	23.20
24		22.67	36.18
24		26.04	67.18
24		27.98	87.36
24		30.76	116.91
24		35.64	160.16
24		43.96	225.04
24		51.78	278.38
24		59.07	328.12
24		67.88	376.42
24			
24		64.45	338.93
24		65.93	354.43
24		68.84	380.02
24		71.78	407.80
24		76.66	454.99
24		81.05	491.46
24		87.42	540.77
24		93.26	588.11
24		98.14	630.15
24		102.07	653.01
24		108.41	692.87
24		112.30	715.04
24		116.72	738.28
24		122.56	764.08
2/29/2008	7:36:46 AM		
25		22.97	22.17
25		29.73	75.64
25		35.81	132.93
25		43.23	189.26
25		49.34	228.41
25		56.76	278.06
25		63.53	320.07
25			
25		60.82	280.33
25		65.54	328.10
25		75.67	394.97
25		84.45	463.75
25		91.91	505.78
25		99.99	544.00
25		108.08	574.56

8		111.54	713.59
8		118.04	742.00
8		124.51	774.20
8		135.14	810.18
8/10/2007	7:33:00 AM		
9		37.26	37.07
9		40.76	71.96
9		47.09	134.27
9		53.43	202.97
9		62.57	291.15
9		73.79	425.48
9		82.24	504.43
9		92.07	602.86
9		104.02	708.48
9		113.85	785.38
9		132.86	887.92
9		148.30	969.95
9		163.78	1036.60
9			
9		157.44	658.77
9		164.47	724.43
9		172.92	800.35
9		182.75	874.21
9		189.78	931.66
9		194.70	958.34
9		202.42	1019.89
9		212.26	1077.34
9		223.51	1136.85
9		232.65	1184.04
9		247.40	1253.80
9			
9		222.12	640.31
9		246.02	814.71
9		271.33	980.91
9		286.77	1079.39
9		293.80	1114.28
9		305.05	1186.09
9		314.89	1239.44
8/29/2007	7:20:00 AM		
10		74.68	37.80
10		77.35	76.48
10		81.35	121.26
10		88.01	184.36
10		92.66	212.86
10		96.00	238.30
10		100.68	281.04
10		104.68	318.70
10		109.33	365.52
10		122.00	460.17
10		134.01	542.61

25			
25		101.24	563.10
25		110.12	620.42
25		115.60	662.45
25		119.72	700.66
25		124.51	729.32
25		134.08	790.46
25		136.82	811.48
25		143.65	851.60
25		151.17	891.72
25		164.18	945.22
25		173.75	991.07
25			
25		127.91	437.00
25		129.99	461.84
25		136.82	526.80
25		142.96	593.67
25		146.39	622.33
25		153.22	677.74
25		157.34	714.04
25		162.82	763.71
25		169.65	809.57
25		179.22	872.62
25		186.75	910.83
2/29/2008	7:53:33 AM		
26		17.29	13.25
26		18.98	33.05
26		20.39	45.63
26		22.18	61.59
26		24.16	81.84
26		26.53	100.61
26		30.53	133.45
26		33.26	153.15
26		34.52	165.35
26		35.48	175.64
26		36.40	184.09
26		37.39	192.56
26		39.20	215.08
26		41.02	234.78
26		44.19	268.56
26		46.50	293.89
26		49.70	327.67
26		54.25	374.58
26		57.65	412.11
26		61.55	467.47
26		65.24	516.26
26		69.27	575.37
26		71.58	610.09
26		73.66	639.18
26		76.56	681.40

10		143.35	591.46
10		153.35	640.78
10		163.35	667.26
10			
10		125.33	397.07
10		130.02	454.06
10		133.35	490.70
10		136.69	520.21
10		140.68	546.68
10		146.69	583.31
10		154.67	618.38
10		162.00	656.59
10			
10		126.69	345.16
10		130.02	388.93
10		135.99	452.03
10		141.34	493.75
10		152.00	577.21
10		165.33	649.47
10		176.68	720.71
10		183.35	755.31
10		190.67	796.02
10		199.35	847.93
10		206.68	886.60
8/31/2007	7:00:03 AM		
11		63.43	26.43
11		69.47	49.47
11		74.51	77.76
11		80.55	108.13
11		83.59	128.04
11		87.62	154.22
11		89.63	169.94
11		93.65	195.08
11		95.67	217.07
11		99.69	251.64
11		104.71	278.88
11			
11		102.70	276.78
11		107.75	328.11
11		110.75	359.53
11		114.77	400.39
11		117.81	428.67
11			
11		123.88	477.90
11		127.88	506.18
11		135.93	570.08
11		145.00	642.36
11		152.03	710.45
11		161.11	771.20
11		168.17	833.01

26		79.76	716.11
26		84.18	764.90
26		87.52	796.80
26		93.42	849.35
26		99.76	888.75
26		107.78	936.61
26		121.41	1007.91
26			
26		107.58	474.98
26		109.43	495.62
26		111.74	522.83
26		113.59	548.16
26		116.82	574.43
26		120.05	610.09
26		124.21	649.50
26		127.45	681.40
26		129.29	700.16
26		132.53	730.19
26		134.38	748.95
26		138.07	783.67
26		142.23	816.51
26		146.85	860.61
26		149.62	882.19
26		152.86	909.40
26		156.06	931.91
26		162.06	974.14
26		167.61	1007.91
26		173.61	1042.63
2/29/2008	9:01:31 AM		
27		25.97	9.44
27		29.11	22.36
27		32.27	39.88
27		37.98	83.24
27		39.24	99.84
27		42.41	132.12
27		44.95	157.95
27		50.03	207.76
27		55.70	246.51
27		58.87	274.18
27		61.41	295.39
27		69.63	355.35
27		75.34	395.02
27		79.13	441.14
27		82.93	475.27
27		89.27	531.54
27		94.97	567.51
27		98.93	594.26
27		102.17	615.48
27		103.46	626.55
27		106.00	642.23

11		179.22	914.71
11		187.28	989.08
11		193.31	1040.41
11		198.36	1098.02
11		204.40	1161.92
11		208.43	1197.54
11		212.45	1228.96
11		215.49	1248.86
11			
11		209.45	1147.26
11		213.48	1190.20
11		218.49	1247.82
11		221.53	1287.62
11		224.53	1323.24
11		228.56	1368.28
11		230.57	1390.28
11		232.58	1414.37
11		238.62	1474.08
11		246.68	1540.07
11		250.73	1578.83
11		257.76	1615.49
11		271.85	1669.96
8/31/2007	8:37:00 AM		
12		44.98	30.38
12		47.69	66.95
12		50.49	100.29
12		51.91	116.42
12		53.30	135.78
12		57.52	184.18
12		58.91	212.14
12		60.32	236.88
12		63.13	275.60
12		67.32	334.75
12		70.13	371.32
12		72.93	401.43
12		77.15	450.91
12		81.35	499.31
12		86.96	535.87
12		92.57	586.42
12		98.04	602.56
12		102.40	658.48
12		105.14	685.37
12		109.40	718.71
12		113.65	760.66
12		127.88	871.43
12		139.23	945.64
12		150.61	1026.31
12		166.22	1120.95
12		184.70	1225.28
12		203.18	1296.26

27		110.52	671.75
27		115.63	704.95
27		121.44	748.31
27		124.64	768.60
27		131.08	804.58
27		135.56	824.87
27			
27		123.35	579.09
27		129.13	634.47
27		137.48	686.15
27		144.57	748.91
27		150.35	806.13
27		157.41	870.73
27		165.76	931.64
3/4/2008	7:54:15 AM		
28		25.74	47.46
28		31.25	112.75
28		35.87	180.88
28		42.01	260.37
28		48.15	312.41
28		51.98	343.64
28		55.04	379.60
28		58.51	419.34
28		60.98	452.46
28		62.90	469.50
28		65.01	502.62
28		92.07	880.18
28		93.59	901.00
28		95.34	925.60
28		97.45	949.26
28		99.53	978.59
28		100.65	989.95
28		102.96	1017.39
28		106.82	1059.97
28		109.92	1086.47
28		113.62	1122.43
28		116.52	1150.82
28		120.38	1182.99
28		126.39	1225.57
28		131.80	1264.37
28		139.56	1318.31
3/11/2008	8:40:00 AM		
29		34.49	36.35
29		36.80	65.19
29		39.86	94.31
29		42.93	128.10
29		46.76	166.89
29		50.59	207.32
29		54.42	258.57
29		57.49	292.78

12			
12		150.61	998.34
12		157.71	1058.57
12		163.38	1097.29
12		169.06	1133.86
12		177.61	1185.48
12		187.54	1250.02
12		197.47	1302.72
12		203.18	1332.83
12		213.11	1372.62
12		221.63	1393.06
12		225.92	1408.12
12		231.59	1437.15
12		237.27	1458.67
12		250.04	1504.91
12		258.59	1535.03
12		268.52	1573.75
12		274.20	1610.31
12		281.33	1643.65
12		298.35	1720.02
12		308.32	1764.11
12		318.25	1810.36
12		322.51	1839.40
12		329.60	1885.64
12			
12		423.39	37.91
12		424.81	57.27
12		427.65	97.06
12		430.49	128.25
12		433.32	159.44
12		436.16	189.56
12			
12		434.74	140.08
12		437.61	186.33
12		439.03	204.61
12		440.45	232.58
12		441.87	257.31
12		444.71	296.03
12		447.55	350.88
12		451.80	421.87
12		454.64	467.04
12			
12		473.12	780.51
12		477.38	840.24
12		484.47	928.44
12		490.18	984.96
12		494.44	1018.78
12		498.70	1068.25
12		505.79	1144.61
12		512.89	1219.90

29		63.62	350.61
29		66.69	393.02
29		70.52	439.15
29		72.83	463.61
29		77.42	516.57
29			
29		44.45	128.10
29		46.76	158.39
29		48.31	173.53
29		50.59	202.66
29		53.66	229.45
29		57.49	273.72
29		59.80	294.69
29		62.11	323.81
29		65.18	359.93
29		67.45	387.89
29		70.52	419.34
29		74.38	447.30
29			
29		69.00	404.20
29		72.83	470.60
29		74.38	495.07
29		78.97	555.65
29		82.04	592.92
29		85.11	630.20
29		88.18	680.30
29		90.45	707.09
29		93.52	751.36
29		97.35	787.48
29		101.08	815.44
29		108.08	860.87
29		114.28	901.64
29			
29		87.71	616.19
29		92.24	658.60
29		95.83	696.28
29		100.29	733.97
29		102.83	764.60
29		107.38	809.35
29		110.39	837.62
29		111.97	844.68
29		114.18	882.37
29		118.97	931.84
29		122.50	967.17
29		125.17	995.44
29		127.51	1026.06
29		131.41	1068.46
29		133.72	1099.09
29		138.40	1146.20
29		143.06	1188.60

12		518.60	1269.04
9/4/2007	8:57:45 AM		
13		6.60	27.72
13		8.48	44.92
13		12.41	76.28
13		16.24	97.53
13		19.11	125.86
13		21.95	168.35
13		24.82	195.67
13		26.73	224.00
13		29.60	255.36
13		34.35	317.07
13		39.14	362.60
13		42.01	382.84
13			
13		32.47	271.55
13		34.35	304.93
13		36.27	336.30
13		38.18	366.65
13		40.10	398.01
13		42.04	430.39
13		45.84	481.99
13		48.68	519.42
13		52.50	561.91
13			
13		44.88	446.58
13		46.76	483.00
13		49.63	524.48
13		51.55	554.83
13		54.42	588.22
13		56.33	612.50
13		60.16	644.87
13		63.95	683.32
13		68.74	719.74
13		73.49	757.17
13		79.23	791.57
13		88.77	840.14
13		100.22	881.62
13		109.16	903.87
13			
13		70.65	680.28
13		76.36	744.02
13		81.15	800.68
13		84.98	837.10
13		89.73	877.57
13		93.56	907.92
13		99.30	957.49
13		105.30	992.91
13		109.20	1017.19
13		115.93	1057.66

29		146.16	1216.86
29		150.05	1256.91
29		157.05	1322.86
29		160.15	1355.84
29		171.04	1454.78
3/25/2008	9:12:00 AM		
30		16.90	20.56
30		18.45	44.08
30		20.76	73.24
30		22.28	92.05
30		26.10	139.08
30		28.41	159.77
30		30.72	186.11
30		32.67	204.92
30		34.25	218.08
30		36.56	237.84
30		38.91	260.41
30		42.01	294.27
30		45.90	333.78
30		49.04	360.11
30		53.69	412.78
30		56.03	438.18
30		57.59	452.29
30		62.27	508.72
30		64.58	534.12
30		66.92	563.28
30		71.61	604.66
30		75.50	636.64
30		80.95	668.62
30			
30		75.50	498.88
30		80.95	551.58
30		87.95	606.16
30		98.04	656.98
30		107.38	707.79
30		119.86	768.02
30		136.19	830.13
30		161.11	903.54
30		179.78	950.59
30			
30		196.91	824.49
30		202.36	864.01
30		209.35	907.30
30		216.35	954.35
30		222.59	992.00
30		229.58	1033.40
30		235.03	1065.40
30		246.71	1114.34
30		270.04	1200.91
3/25/2008	9:37:00 AM		

13		123.68	1095.09
13		134.31	1128.48
13		142.99	1154.78
13			
13		89.73	630.71
13		97.38	703.55
13		103.39	755.15
13		111.11	811.81
13		115.50	853.29
13		128.50	922.08
13		134.31	962.55
13		145.89	1026.29
13		151.70	1063.73
13		156.52	1098.12
13		166.19	1148.71
13		174.87	1188.17
13		188.40	1229.65
9/4/2007	9:57:00 AM		
14		119.30	423.12
14		123.88	492.33
14		131.54	602.25
14		142.23	730.50
14		149.89	797.67
14		159.82	893.34
14		165.96	968.66
14		176.65	1090.80
14		183.55	1149.83
14		193.48	1214.97
14		212.59	1335.07
14		228.66	1434.81
14		247.01	1516.23
14		261.53	1573.23
14			
14		202.65	824.13
14		212.59	899.45
14		225.59	995.12
14		262.32	1198.68
14		273.77	1255.68
14		292.12	1341.17
14		315.84	1436.85
14		342.61	1493.84
14			
14		312.02	1003.27
14		329.60	1088.76
14		342.61	1147.79
14		352.54	1186.47
14		370.13	1247.54
14		392.30	1298.43
14		412.20	1343.21
9/8/2007	7:56:00 AM		

31		11.12	17.96
31		12.74	43.65
31		14.32	66.48
31		15.68	79.79
31		18.45	113.09
31		21.22	146.38
31		23.96	182.53
31		25.81	211.07
31		27.03	234.85
31		29.50	264.34
31		31.35	287.17
31		33.17	310.00
31		34.45	326.17
31		35.94	345.20
31		38.18	369.93
31		41.48	405.13
31		44.52	436.52
31		49.76	488.84
31		54.09	524.04
31		59.90	571.60
31		63.62	596.34
31		69.14	624.87
31		73.72	648.66
31		81.11	697.17
31		84.78	728.56
31		89.60	761.86
31		94.35	795.15
31		104.74	856.03
31		116.13	896.86
31		133.75	989.21
31		143.35	1022.53
31		153.75	1056.81
31		167.90	1117.74
31		179.22	1171.06
999	999	999.00	999.00

15		72.27	32.61
15		75.83	68.97
15		77.98	86.00
15		79.40	102.24
15		81.54	120.81
15		83.00	137.06
15		84.41	157.95
15		85.83	178.06
15		88.01	203.59
15		90.16	235.31
15		93.72	261.62
15		96.59	300.30
15		98.74	322.74
15		100.16	341.31
15		100.88	354.72
15		103.03	386.95
15		104.45	403.97
15		106.59	424.86
15		109.46	451.17
15		112.33	486.76
15		114.48	507.65
15		118.04	535.50
15			
15		97.28	288.70
15		99.43	323.51
15		101.57	359.10
15		104.45	402.43
15		108.04	449.62
15		110.88	486.76
15		112.33	516.16
15		114.48	563.35
15		115.90	591.98
15		118.04	632.21
15		120.91	674.76
15		124.48	734.33
15		126.62	769.92
15		130.22	824.08
15		132.36	860.44
15		140.94	966.44
15		145.96	1013.63
15		151.67	1060.05
15		154.54	1093.32
15		158.83	1142.83
15		162.39	1180.74
15		165.99	1217.11
15		170.28	1255.02
15		177.41	1320.00
9/18/2007	8:32:40 AM		
16		43.63	11.19
16		47.06	27.90

16		49.93	41.83
16		52.21	55.75
16		54.52	66.20
16		58.54	83.60
16		61.97	105.89
16		64.28	119.12
16		66.56	134.43
16		71.15	162.98
16		74.02	188.05
16		76.89	214.51
16		78.61	237.49
16		80.32	256.98
16		82.07	273.70
16		83.79	290.41
16		85.50	308.51
16		88.94	341.93
16		92.40	370.48
16		95.83	402.51
16		98.70	426.19
16		101.11	447.08
16		104.45	471.45
16		108.08	499.99
16			
16		133.09	607.23
16		135.99	626.72
16		142.96	660.14
16		150.51	708.19
16		156.92	745.09
16		167.38	796.62
16		175.49	836.31
16		185.39	879.48
16		197.57	931.01
16			
16		129.00	117.03
16		134.84	156.02
16		140.65	194.32
16		145.30	223.56
16		153.42	272.30
16			
16		231.10	32.77
16		235.06	55.75
16		238.43	82.21
16		241.26	105.89
16		245.19	140.01
16		250.27	181.09
16		252.52	206.85
9/27/2007	7:46:59 AM		
17		61.51	36.11
17		64.78	66.93
17		68.81	103.91

17		91.48	293.97
17		97.15	350.48
17		105.77	406.98
17		109.03	424.45
17		114.77	455.27
17		122.17	502.52
17		131.18	558.00
17		142.66	615.53
17		150.84	649.44
17		161.50	683.34
17		179.55	715.19
17		192.65	739.84
17			
17		199.22	668.95
17		201.70	698.75
17		204.14	723.40
17		208.23	774.77
17		212.36	823.06
17		217.27	879.56
17		220.54	917.57
17		223.81	952.50
17		227.11	991.54
17		232.02	1035.72
17		237.77	1090.17
17		240.21	1115.85
17		246.77	1165.16
17		252.52	1202.15
17		258.26	1242.21
17		268.92	1301.80
17		274.66	1337.76
17		283.67	1386.04
17		289.41	1425.08